DIRECT ELECTROCHEMICAL ANALYSIS OF THE REDOX ACTIVITY OF TRYPTOPHAN AND TYROSINE IN MODIFIED AZURINS: THE IMPACT OF THE PROTEIN ENVIRONMENT

by

Kristin Janell Tyson

May, 2021

Director of Thesis: Adam R. Offenbacher, Ph.D.

Major Department: Chemistry

Abstract

Proton-coupled electron transfer (PCET) is a biological process essential to life. It is imperative for respiration in animals as well as photosynthesis in plants. Long-range PCET is often facilitated by redox-active amino acids, such as tryptophan and tyrosine. While there are several examples in the literature for the involvement of these redox-active residues in PCET linked to biological catalysis, there has been a challenge in direct electrochemical efforts to resolve how the local protein environment controls PCET directionality. This thesis describes a protocol from which to directly test the reduction potentials of tyrosine and tryptophan radicals in a customizable protein environment. The model protein used for this study was azurin, a natural cupredoxin that natively contains two tyrosines and only one tryptophan, with the former mutated to phenylalanine to provide direct electrochemical detection of a single redox-active amino acid species. The reduction potentials of azurin with either tryptophan or tyrosine redox centers were monitored using the electrochemical technique square-wave voltammetry. Using this technique along with

strategic protein engineering, it was found that the more solvent-exposed or polar mutants had a higher redox potential than those that were more solvent-excluded. These trends have biological importance as the difference in the reduction potentials between redox-active amino acid pairs is expected to control the thermodynamic driving force for PCET. This thesis details the impact of altering the surrounding protein environment, i.e. electrostatics, on the redox activity of tryptophan and tyrosine.

DIRECT ELECTROCHEMICAL ANALYSIS OF THE REDOX ACTIVITY OF TRYPTOPHAN AND TYROSINE IN MODIFIED AZURINS: THE IMPACT OF THE PROTEIN ENVIRONMENT

A Thesis

Presented To the Faculty of the Department of Chemistry

East Carolina University

In Partial Fulfillment of the Requirements for the Degree

Master of Science in Chemistry

by

Kristin Janell Tyson

May, 2021

DIRECT ELECTROCHEMICAL ANALYSIS OF THE REDOX ACTIVITY OF TRYPTOPHAN AND TYROSINE IN MODIFIED AZURINS: THE IMPACT OF THE PROTEIN ENVIRONMENT

By: Kristin Janell Tyson

APPROVED BY:

DIRECTOR OF THESIS	Adam R. Offenbacher, Ph.D.
COMMITTEE MEMBER	Eli G. Hvastkovs, Ph.D.
COMMITTEE MEMBER	Patrick J. Horn, Ph.D.
COMMITTEE MEMBER	Robert M. Hughes, Ph D.
COMMITTEE MEMBER	Andrew Sargent, Ph.D.
CHAIR OF THE DEPARTMENT OF CHEMISTRY	Andrew T. Morehead, Jr., Ph.D.
DEAN OF THE GRADUATE SCHOOL	Paul Gemperline, Ph.D.

This Thesis is Dedicated to

My Amazing, Loving Brother

Joshua Charles Tyson

“Your value stays constant whether it is seen or not.” - SEEKER

ACKNOWLEDGEMENTS

There are so many people who helped to bring this thesis together that I fear I do not have enough time nor space to thank everyone. Instead, I will try to keep it brief and encourage everyone to recall memories of the happy times that occurred throughout this journey. I suppose I should start off by thanking those who gave birth to me, Mama and Daddy. The two of you have been there for me through good times and bad; times when I wondered if I was enough good enough, smart enough, or determined enough to be a chemist. It was not the direction you saw me going in college, but I hope I made you both proud. (Maybe I can get my Ferrari now, at least.) To my awesome brother to whom this thesis is dedicated to, Joshua...well, you have this huge hunk of sleepless nights, tears, laughter, and hysteria dedicated to you. That should be enough. Hahaha. I would also like to mention my Aunt Jo-Ellen and my grandparents, Nana and Granddaddy, for understanding my struggle to a tee and listening enthusiastically while I confuse them, respectively. To my family, I love you all so much.

I suppose now it is time to thank my chemistry peeps. It is arguable that this thesis would not have come together without the encouragement and persistence of my best friends, Amy and Caitlin. I love you both to infinity. A huge thanks also to Dr. Adam Offenbacher who always stepped in right as I was ready to give up and made me realize the failures were just as important as the successes. And thanks to my fellow lab members, both new and old. You all saw me at my best, and at my worst, and still chose to stick around to see how well I could steer this crazy ship. I hope I made you all proud.

And to little ole me, Kristin Janell Tyson. You did a good job, girl. You deserve to give yourself a round of applause and a chocolate donut. No sprinkles, though.

TABLE OF CONTENTS

LIST OF TABLES

LIST OF FIGURES

LIST OF EQUATIONS

LIST OF SYMBOLS OR ABBREVIATIONS

CHAPTER 1: Introduction

1.1 The Biological Importance of Proton-Coupled Electron Transfer

One can argue that everyday life is simply a compilation of various reactions that are occurring throughout the universe. Science encompasses the study of many said reactions, including mechanisms that are imperative for biological function in nature and in the human body. An example of one such mechanism is electron transfer. Electron transfer (ET) reactions are a central part of multiple catalytic activities and processes, including energy conversion in oxygen respiration and photosynthesis.[1] In simplistic terms, photosynthesis is the process by which plants absorb light in the form of photons and convert it to chemical energy. This energy, along with carbon dioxide, is then used by the plants to synthesize sugar in the form of glucose. Glucose is a usable source of potential chemical energy; thus, photosynthesis provides metabolic energy for biological systems to use. ET is especially prevalent in the chlorophyll molecules within the enzyme photosystem II that converts water to molecular oxygen as the Earth's source of atmospheric oxygen. Water oxidation in photosystem II is coupled to reduction of membrane-embedded quinone electron carriers used for carbon dioxide fixation. Two light-driven proton pumps, photosystem I and II, are responsible for generating a proton gradient that eventually provides energy to create ATP and NADPH, two essential energy storing chemicals and carrier molecules for cells. These processes are achieved through mediation and control of electron transfer.[2,3] In biological reactions, electron transfer is often coupled to the transfer of protons in a proton-coupled electron transfer (PCET) process. These reactions are considered to be highly regulated by the acidity of the proton at the donor by the local protein environment.

1.2 Amino Acids Involved in Electron Transfer and RNR as a Case Study

Amino acids (AAs) are known to be involved in ET mechanisms and are particularly important in directing the moving electron. Upon the loss of an electron, a radical will form on the AAs. However, not all amino acids are able to directly control electron transfer. Tyrosine (Y) and tryptophan (W) are cyclic aromatic amino acids that play important roles in biological ET. For example, the very important catalytic protein, ribonucleotide reductase, requires multiple amino acids, including tyrosine, tryptophan and cysteine, to assist in its long-range electron transfer process that is coupled to catalysis. Ribonucleotide reductase (RNR) catalyzes the reduction of ribonucleotides to deoxyribonucleotide monomers, and it does so with a high efficiency without the generation of reactive oxygen species (ROS). In all RNRs, substrate reduction is initiated by a C-H bond cleavage at the ribose 2' carbon by a transient thiyl radical at a conserved cysteine residue. The class Ia is the most well studied enzyme class and encompasses human and bacterial RNRs. In this class, the transient thiyl radical in the catalytic α2 subunit is generated by a stable tyrosyl radical, adjacent to a differic cluster in the β2 subunit. Upon transient formation of the α2β2 complex from substrate binding in α2, the tyrosyl radical in β2 is separated from the cysteine residue in α2 by 35 Å. From Marcus theory that describes the transfer of electrons by quantum mechanical wavefunction overlap (see section 1.3), an electron generally travels a maximum distance of 15 Å. This distance is limited by its de Broglie wavelength. How does an electron travel 35 Å in RNR? It is believed that the electron undergoes a hopping mechanism, involving several amino acid side chains. There are three tyrosine residues and one tryptophan that are intrinsically involved in this process (**Figure 1.1**).[4-8] While the involvement of these AAs in ET have been demonstrated, it is not clear what is the basis for the control of ET directionality. In RNR, once radical transfer occurs on the forward pathway to generate the cysteine radical and chemistry takes

place, reverse ET must occur to regenerate the stable tyrosyl radical in β2. How the local protein environment controls this directionality of ET is not well understood but is likely to arise from altered thermodynamics of ET that are controlled by local hydrogen bonding interactions. This thesis seeks to address how the local protein environment may control the reduction potentials of protein-based amino acids that is linked to the ET driving force.

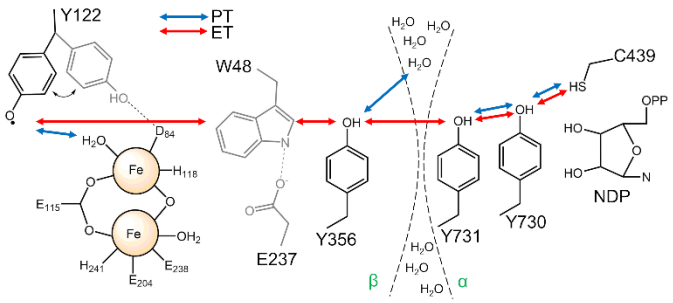

Figure 1.1. Diagram of PCET pathway for radical transfer from Y122 in β2 radical to C439 in α2. (*Image courtesy of Dr. Adam R. Offenbacher.)*

1.3 Marcus Theory that Describes Electron Transfer

Many chemists are aware of the general description of a chemical reaction. That is at its most basic, a chemical reaction involves a reactant that must overcome an energetic 'hill' to produce a product. The difference between the reactant well and the peak of the hill – referred to as the transition state - is known as the activation energy (E_a). Other parameters can be found such as the Gibbs free energy of the reaction ($\Delta G°$) which reflects the energetic difference between the reactant and product wells. However, this way of describing a chemical reaction is based on classical transition state theory and cannot explain the transfer of electrons that occurs quantum mechanically.

The movement of electrons and protons coupled to electron transfer is well described by Marcus theory. Marcus theory was originally introduced in 1956 by Rudolph A. Marcus. His work was done during a time at which the early stages of quantum mechanics were being born and electron transfer reactions were crucial and needed to be studied.[9] Marcus realized that the rate of ET was dependent upon the $\Delta G°$ for the reaction and an additional term, the reorganization energy (λ). Further, instead of treating electrons as particles, the theory allowed for the transfer of electrons to be understood by their 'wave-like' properties. λ is defined as the energy needed to reorganize/reorient the nuclear configurations of the reactants to enable degeneracy of the wave functions of the reactants and products (**Figure 1.2**).[10] The reorganization energy can be found by comparing the distance between dD (point on the GA parabola at which the reactant well is at its lowest value) and dA (the bottom of the product well).[11] In this instance, unlike the classical transition state theory, there is no transition state in Marcus theory. The main energetic barrier in Marcus theory is λ.

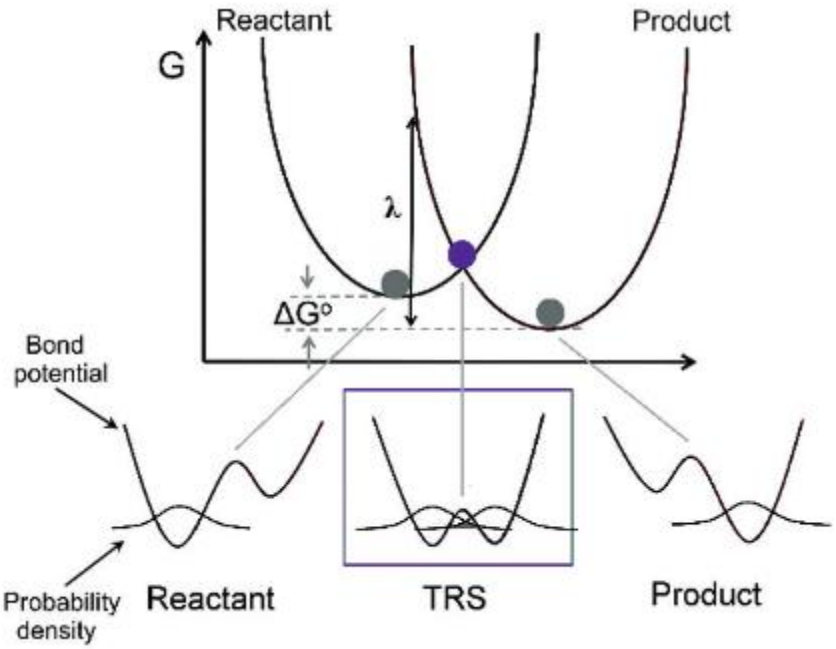

Figure 1.2. Graphical representation of the Marcus reaction coordinate involving the heavy atom positions (top) and defined by λ and the driving force, ΔG°. At the TRS (purple dot), the positioning of the electron wavefunction (bottom) has become energetically degenerate across the reactant (donor) and product (acceptor) wells. Figure reproduced from Whittington *et al. 2020*.

When applied to an electron transfer reaction, the two main variables to examine are ΔG° and λ. The two are directly related, so when changes occur in ΔG°, λ is also affected. When λ changes (i.e., conformational change), the parabolas shift horizontally, resulting in a larger activation energy barrier. While λ is the main determinant for the PCET rates, ΔG° is considered to control the directionality of electron transfer. In the case of protein amino acid radicals, the ΔG° is related to the difference in the reduction potentials (E_{cell}°) between the electron donor and acceptor:

$$\Delta G^{\circ} = -nFE^{\circ}_{cell} \qquad \textbf{\textit{Equation 1.1}}$$

where *n* is the number of electrons, F is the Faraday constant and $E_{cell} = E_{ox} + E_{red}$. A further explanation of the relationship between ΔG and the potential energy (E) is defined by the Nernst equation. The Nernst equation describes the relationship between cell potentials and activities of the cell under non-standard conditions:

$$E = E^{\circ} - (\frac{RT}{nF})(lnQ) \qquad \textbf{\textit{Equation 1.2}}$$

The potential difference (E) is directly related to the standard reduction potential (E°). R is the gas constant, and T refers to the temperature at which the reaction is occurring. When the temperature is held at 298 K, the Nernst equation can be simplified as follows:

$$E = E^{\circ} - (\frac{0.059}{n})(\log_{10} Q) \qquad \textbf{\textit{Equation 1.3}}$$

At this moment during the reaction, Q is defined as the ratio of the concentration of products over the concentration of reactants. Amino acids that are redox active (lose electrons) have acidic character. These oxidation reactions of an amino acid (AA) would be noted as $[HAA] \rightarrow [H^+] + [AA^-]$. When transitioning by a pH unit, the $\log_{10}Q$ term in the above Nernst relationship reduces to ΔpH. Thus, within the pH dependent regime, for every 1 pH unit change, there will be a 59 mV change in the potential. For example, as the pH experiences a +1 change, the reduction potential for an amino acid will decrease by 59 mV.[12]

There are multiple variables that impact the observed reduction potentials of amino acids. Amino acid side chains are generally acidic which will result in an impact on the pH-dependency of the overall system. Changes in the acidity constant thorough space non-covalent interactions can influence the potentials until the pK_a is reached, at which point the amino acid side chain is deprotonated and thus the potential is pH-independent (i.e., there is no proton to lose). And while

the Nernst equation can be used to derive many important parameters regarding electron transfer, the standard potentials observed in solution do not illuminate the complexities (i.e. influence of non-covalent interactions) arising from a protein environment. In order to detect how the local protein environment influences amino acid reduction potentials, electrochemical techniques are used on small model protein (or biomimetic) systems.

1.4 Electrochemical Analysis Techniques

Electrochemistry refers to the science relating electron movement to chemical changes.[13] In the context of this thesis, electrochemistry is used to directly detect the potentials of amino acid radicals, tyrosine and tryptophan, and examine how the peptide and protein environments can alter them. To achieve this, an instrument known as a potentiostat was used. Some potentiostats can work with 4-electrode, 3-electrode, or 2-electrode setups. This project involves a 3-electrode system (**Figure 1.3**). One of the electrodes was a working electrode. The working electrode was a pyrolytic graphite (PG) electrode which allowed current to flow through it uninterrupted to the species of interest. A second electrode, the counter electrode, was a platinum electrode whose function was to complete the path of the current in the cell. The third electrode, known as the reference electrode, was a standard calomel electrode (SCE). The SCE contained the inert chemicals Ag/AgCl. It was stable and held a constant potential during experimentation. Thus, the SCE provided the standard against which to base the potential change measured at the working electrode. This 3-electrode setup was chosen due to it measuring only one half of the electrochemical cell, allowing for the measurement of current at the working electrode as a function of potential.[14]

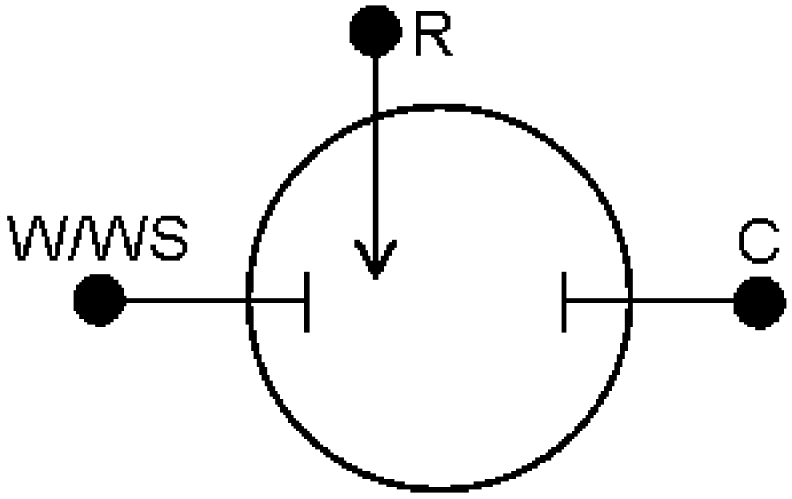

Figure 1.3 Electrochemical cell setup of a 3-electrode system. W/WS denoted the working electrode. C denoted the counter electrode, and R denoted the reference electrode.[14]

Two electrochemical analysis techniques that were used in this project were cyclic voltammetry (CV) and square wave voltammetry (SWV). Cyclic voltammetry (CV) refers to the method of probing a system in a cyclic fashion. Voltages sweep multiple times over an imposed x-axis at a specified rate, typically sweeping first in the positive direction (oxidation) then following back in the negative direction (reduction). The resulting current (i) produced was plotted as can be seen below (**Figure 1.4**). The current observed in the beginning of the sweep, closest to the y-axis, is known as the capacitive current. The sharp increase seen is the Faradaic current, the signal denoted by ET from the electrode to the analyte. Averaging the collected currents resulted in a peak corresponding to the oxidation (anodic) and an inverted peak corresponding to the reduction (cathodic). The potential value that related to the highest and lowest points of the peaks after background subtraction determined the oxidation and reduction potentials of the analyte. It was used primarily for smaller systems such as peptides and shorter polymers. It has limitations in

its inability to deeply probe larger systems such as proteins and polypeptides. As a technique, it was not sensitive enough to detect buried redox potentials. CV worked better for small molecules where there was no complex environment surrounding the redox species to overcome. Due to these limitations, a more sensitive analysis method was required.[15]

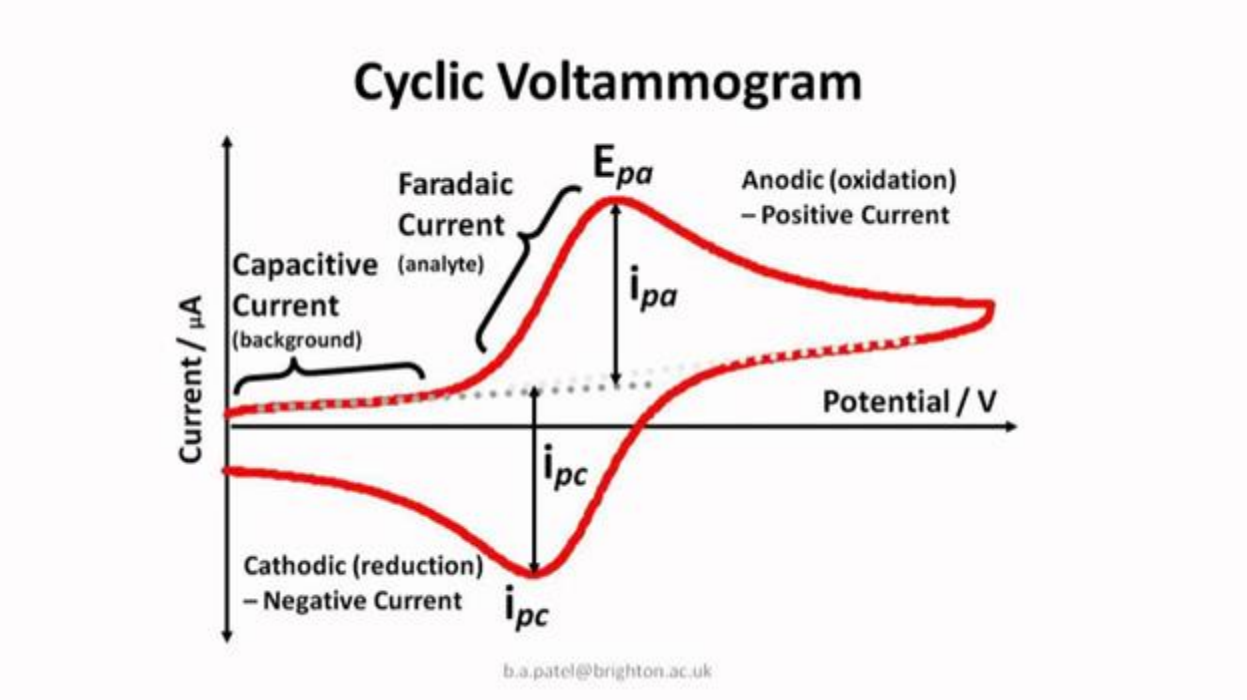

Figure 1.4. Diagram of a typical CV in which the i_{pa} and i_{pc} represents the peak anodic and cathodic current, respectively, for a reversible reaction.[16]

To probe larger and more complex protein systems such as azurin, square-wave voltammetry (SWV) is required. It is a newer, highly sensitive technique that is often used to probe higher ordered systems. It begins with the initial voltage increasing to a set point before being held constant. At this plateau, the "forward" current (I_{for}) is measured. The voltage is decreased to slightly less than the initial voltage, held constant, and the "reverse" current (I_{rev}) is measured. This reoccurring alteration of potential is repeated over the time at the chosen frequency (**Figure 1.5**).

Higher frequencies are often required to probe deeper systems; however, this will be costly as the noise will also increase. The resulting current is plotted as the difference between the I_{for} and I_{rev}. By performing this subtraction, the non-Faradaic current is eliminated, isolating the current associated with the electron transfer. The remaining Faradaic current has a direct relationship with the energy required for electron transfer and can be observed as a peak in the spectrum.[17]

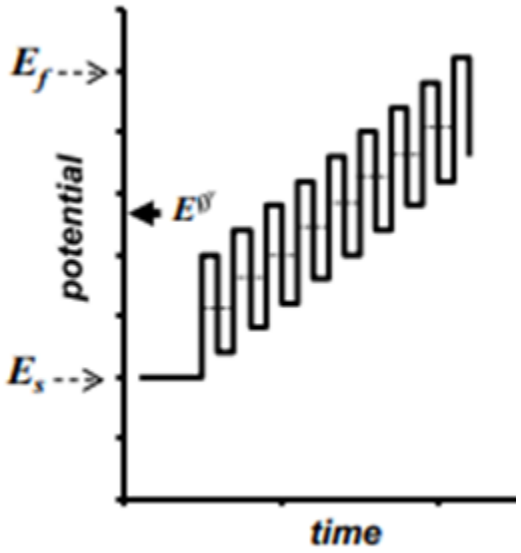

Figure 1.5. Diagram depicting the current flow in square-wave voltammetry. The current is held steady and then increased immediately from 0→1. The "forward" current is measured. It drops immediately, though to a lesser extent, at which point the "reverse" current is measured. The process then repeats until the end voltage is reached. The difference between these currents, the net current, is used to determine the oxidation potential.[6]

Electrochemical analysis techniques can also determine the reversibility of the system being analyzed. Some systems are reversible while other are either quasi- or non-reversible. To determine the reversibility of the system, the ratio of I_{for} to I_{rev} currents are calculated. A ratio of 1 is a completely reversible system. Reversibility, or lack thereof, is important when deciding whether the currents being observed are a true reflection of what is occurring in the system. If a

system is found to be reversible, then the currents and subsequent peak potentials that are observed can be trusted as accurately describing what is occurring. If a system is not reversible, however, what the potentiostat is reading does not truly reflect the potential of the redox event.

After determining the best method of analysis, the protocol for preparation of the working electrode must be determined. There were two commonly used methods: the redox active species can be prepared in solution or it can be immobilized directly onto the electrode surface. To perform a measurement in solution meant that it was dissolved in some type of inert buffer solution. The three electrodes could then be lowered directly into the solution containing both analyte and buffer, and the potential could be measured. As mentioned before, solution studies were typically used to detect small molecule species that directly interacted with the electrode. Large molecules were not ideal for solution studies often due to their inability to fully dissolve in solution as well as their lack of affinity toward the electrode. It was difficult to ensure they were close enough to the electrode surface to accurately be measured. For this thesis project, solution studies were performed to determine limitations before protein work was started. The results provided information regarding the best buffer to use over an extended pH range.

The second way to prepare the working electrode was to attach the redox active species directly to the electrode surface. This method was used when working with larger systems that are difficult or impossible to dissolve in buffer, such as proteins. Proteins typically contain buried redox centers, and as such, they need to be immobilized on the electrode surface to increase the signal enough to measure it. There are multiple ways to immobilize the species onto the electrode surface that span degrees of complexity. Some of the simpler methods involve direct adsorption and layer-by-layer (LBL) adsorption (**Figure 1.6**). Direct adsorption involves adsorbing a redox

protein sample directly to the electrode surface. The surface of the electrode is typically some lipophilic material, allowing for the protein to create a sort of film over the surface and thus be close enough to measure a signal. This method is often used when analyzing the activation of an enzyme in the presence of a substrate. It is incredibly useful when monitoring ion exchange and catalysis reaction.[18,19] The LbL method is used for proteins that do not undergo ion exchange or catalysis but rather ET within itself. LbL also negates the need for creating a protein film. Instead, it relies on the attraction between polymers with different charges to attach a protein close to the electrode surface.[20]

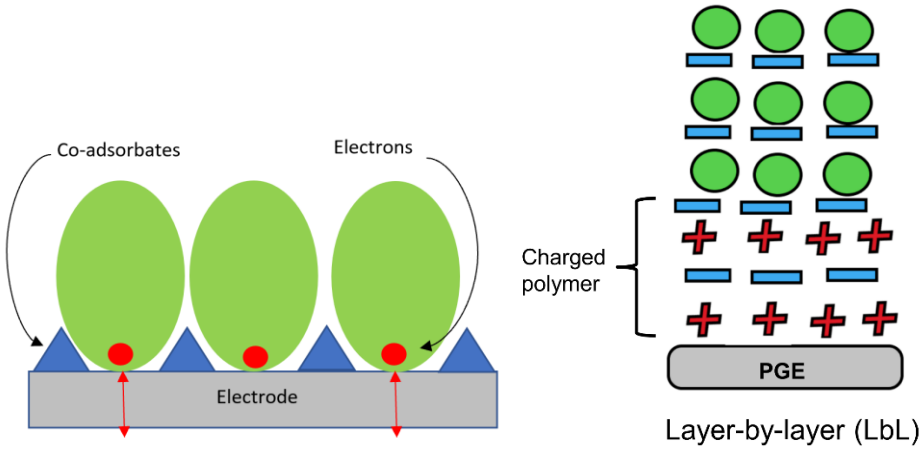

Figure 1.6. Diagrams depicting preparation when following the protein thin-film immobilization (left) and the layer-by-layer (right) methods. The protein is represented in green ovals. (*Image courtesy of Kristin Tyson.)*

1.5 Past Work that Inspired this Thesis

1.5.1 Biomimetic β-hairpin Peptides

PCET is an essential reaction in enzyme mechanisms, several of which directly involve tyrosine. As previously discussed, the role of tyrosyl radical oxidation in biological systems is incredibly important. The role of tyrosine and tryptophan radicals has been extensively studied, and their catalytic applications have been discussed in multiple enzymatic systems.[21-25] However, the majority of these studies described the overall impact of the oxidation and subsequent formation of tyrosyl radicals. There is a lack of information regarding the impacts that environmental changes could have on the reduction potential, and subsequent reactivity, of the radicals. The lack in information is due, in part, to the complexity of the systems that prevent direct electrochemical determination of the reduction potentials for the specific amino acid radical that is linked to the driving force for the rate of ET.

To overcome these limitations, there are two groups that have determined the reduction potentials of tyrosine and tryptophan in simplified, defined (poly)peptides. First, a group led by Bridgette A. Barry investigated this area to explore the influence of environmental factors on the structure and function of tyrosyl radicals as they relate to proton and electron coupling, focusing on cross-strand aromatic, π-cation, hydrophobic interactions in a biomimetic, β-hairpin peptide.[26]

Tyrosine oxidation is known to occur on the aromatic ring, generating a neutral radical. At neutral pH values, the oxidation of a neutral tyrosine is coupled with the deprotonation of the phenolic oxygen.[27] This PCET reaction is due to a decrease in the pK_a of the phenolic oxygen, resulting in changes in the pK_a that can directly impact the free energy of the PCET reaction.[28] In addition to altering pK_a, the potentials of a nearby redox-active cofactor can influence the rate of electron transfer, according to Marcus theory.[29] Redox potentials can be influenced by the hydrophobicity of the surrounding environment (specifically polarity and presence or absence of

hydrogen bonding) and the shielding of potential proton acceptors by large amino acid side chains. Intermolecular interactions often cause a shift in the midpoint potential, or the potential at which the activity of the reductant and oxidant are equal during a redox titration.[30]

To probe the role of intermolecular and covalent interactions on reduction potentials and by extension the PCET rates, peptide systems or small model proteins (<5 kDa) have been typically utilized. As a first example, the Barry group designed an 18 amino acid peptide (**Figure 1.7A**) that contained a single tyrosine residue (Y). The peptide was designed to fold into a β-hairpin polypeptide that enables interstrand hydrogen bonding between Y and histidine (H) residues; this peptide was referred to as 'peptide A'. In addition to His, there were two salt bridges present, and the turn was facilitated by the asparagine (N) and glycine (G) amino acids. The β-hairpin conformation was validated by NMR spectroscopy at pH 5.0 (**Figure 1.7B**) which also showed multiple points of dipolar contact between the cofacially aligned Tyr5 and His14 (**Figure 1.7C**). The group probed the impact of the cross-strand interactions by way of electrochemistry.

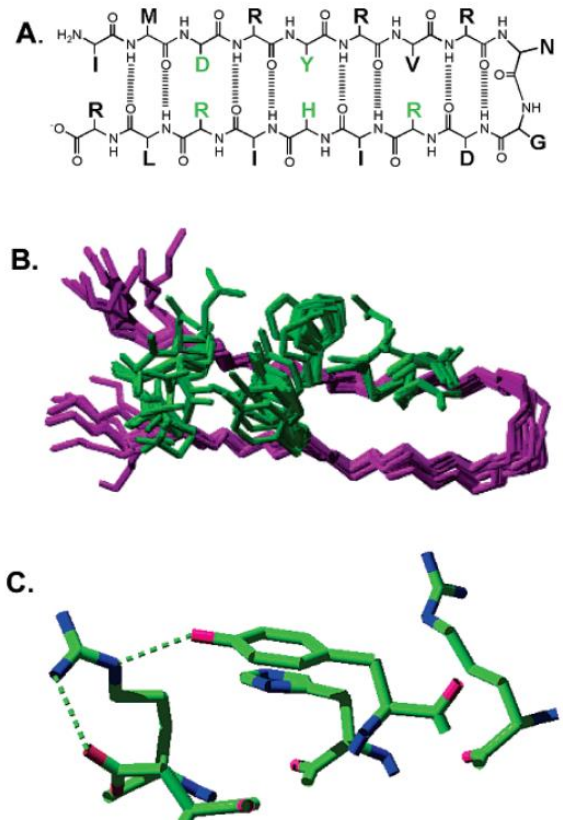

Figure 1.7. A. Primary sequence of peptide (IMDRYRVRNGDRIHIRLR) synthesized by Barry group with predicted hydrogen bonds and cross-strand interactions highlighted in green. B. Overlap of the 20 lowest energy structures as determined by 2-D NMR at pH 5.0. C. Tyrosine, Tyr5, interactions as determined by NMR structure. Hydrogen bonds are shown as dotted lines.[26]

Uncorrected potentials, as measured by SWV, are shown in **Table 1.1**. They measured the peptides in different buffers which produced similar results, and they monitored the potentials as a function of pH. The potentials of the tyrosine solutions linearly increased as the pH of the solutions decreased (1.02 ± 0.01 at pH 5.0 versus 0.70 ± 0.01 at pH 11.0). The same trend could be seen for Peptide A (0.97 ± 0.01 at pH 5.0 versus 0.69 ± 0.01 at pH 11.0), with very little difference in the potentials between Tyr in solution and in peptide A, at these pH values.

Table 1.1. Electrochemical Studies of Peptide A and Tyrosine Samples[26]

Sample	pH	Peak Potentials (V vs NHE)
Peptide A	5.0	0.97 ± 0.01
Tyrosine	5.0	1.02 ± 0.01
Peptide A	11.0	0.69 ± 0.01
Tyrosinate (Y-O•/Y-O-)	11.0	0.70 ± 0.01

The raw electrochemistry data for the tyrosine solution and peptides were graphed (**Figure 1.8**). The raw slopes of the data were discovered to be 63 mV/pH unit which is consistent with the expected slope according to the Nernst equation (59 mV/pH unit). The lines were then fit to model the Nernst equation with the understanding that a single proton was being transferred. The tyrosine solution was observed to decrease linearly until it hit the pK_a of the phenolic oxygen (10.0). Peptide A, however, had a more complex reaction. Rather than having one inflection point, there were two (7.0 and 8.0), indicating that the cross-strand His14 was having dipolar contacts with Tyr5 (**Figure 1.7B-C**). The pK_a values of 10 and 0 were attributed to the reduced and oxidized state of Tyr5, whereas the values of 4.0 and 4.5 were attributed to the reduced and oxidized state of Asp3, respectively. To confirm that these inflection points were indeed the result of dipolar contacts, the Barry group studied Peptide C. Peptide C was the same backbone as Peptide A with the exception of a single mutation: His14 was substituted for cyclohexylalanine. This allowed it to act as a control for measuring the interactions between the Tyr5 and His14. With the dipolar contact now gone, there were no observable inflection points in the graph. The slope changes that were present were attributed to the reduced and oxidized state of His14X.

These values were significant due to the normal pK_a of histidine in protein being 7.0. The pK_a value of histidine in Peptide A was around 1 pH unit higher. This increase indicated that, between pH 7.0 and pH 8.0, the oxidation of tyrosine resulted in a net transfer of a proton from

Tyr5 to His14, resulting in the protonation of His14. This hypothesis was further supported by the similar slope values between pH 8.0-10.0 and pH 4.5-6.9. The slope values were 51 ± 9 mV/pH unit and 53 ±3 mV/pH unit, consistent with a single proton-single electron transfer. In conclusion, during a PCET reaction, a single proton accompanies the oxidation of Tyr5 within Peptide A. The consequences of this reaction seem to favor the formation of a tyrosyl radical at a low pH which can be determined by comparing Peptide C to Peptide A from a peak potential standpoint. The tyrosyl radical was stabilized by the interstrand π-cation interaction with His. The Barry group suggested that the oxidation of the tyrosine and protonation of the histidine in Peptide A are thermodynamically linked. Even though the two amino acids were not directly hydrogen bonded, the peptide bond formation and proton transfer linked the two and resulted in an altered redox potential of tyrosine.[26]

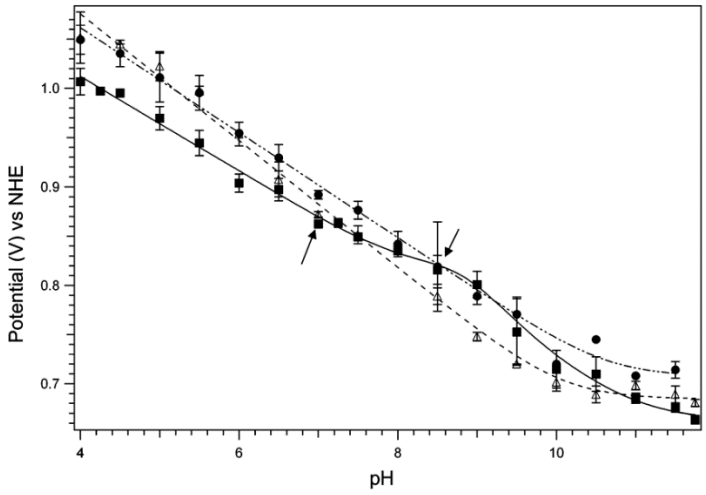

Figure 1.8. SWV measurements of the anodic waves to determine the effect of pH on peak potential. Peptide A is depicted as the black squares, Peptide C is the black circles, and the tyrosine solutions are the open triangles. The data were fit to an oxidation model coupled to the protonation of one (dashed line) or three (solid line) ionizable groups.[26]

New peptides were designed that exhibited different hydrogen bonding and/or π-cation interactions.[31] Hydrogen bonding and other factors, such as distance, are well known to impact the rate of electron transfer. Studies of phenol derivatives have shown that hydrogen bonding will drastically alter the redox potential of tyrosine.[28] To obtain results regarding the impact of these changes, various peptides were synthesized with substitutions made at His14, Arg12, and Arg16. The sequences for these amino acids and predicted interactions are shown in **Figure 1.9**. Each peptide contained only one tyrosine with at least one salt bride, a Asn-Gly turn, and several amino acids that are likely to form a β-sheets. For Peptide F, Arg12 was mutated to Ile to demonstrate π-cation interaction while Arg16 was mutated to Ile to demonstrate hydrogen bonding in Peptide E.

The stabilities of these peptides were measured by CD at pH 5.0, confirming the formation of β-hairpins. Peptide A was used as a control for what the remainder of the peptides should look like, as NMR studies were done that also supported the hypothesis of a β-hairpin structure. When similar thermal denaturation was observed for Peptides C-F as was observed for Peptide A, the Group concluded that Peptides C-F did in fact fold similarly to that of Peptide A.

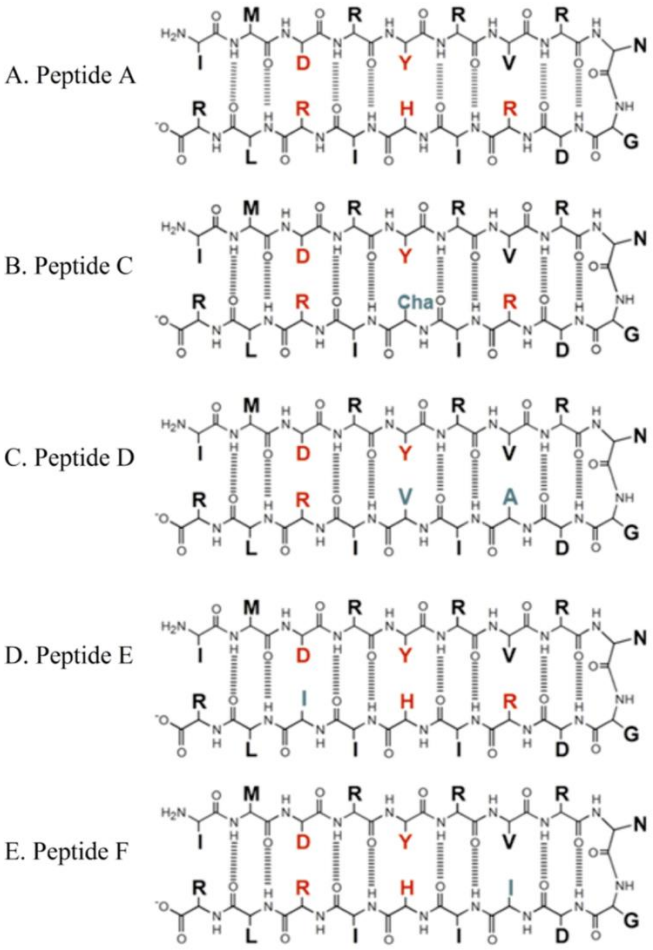

Figure 1.9. Sequence of Peptide A and Peptides C-F with predicted β-hairpin structures and cross-strand interactions. Amino acids involved in interactions are shown in red with mutations in sequence shown in green. Peptide B was excluded from this study as the CD structure indicated the formation of a random coil.[31]

Upon confirmation of stability and overall structural folding, electrochemical titration experiments were performed for each peptide. As can be seen in **Figure 1.10**, the reduction potentials for tyrosyl radical were plotted against pH for the various peptides, with Peptide A acting as a comparison. The titration of tyrosine in solution was used as a control (**Figure 1.9**), as the linear dependence of pH below the phenolic pK_a was observed. The other peptides had amino acids

that were expected to show pK_a shifts which would show in the pH range of the titrations, reflecting the pH dependence of said peptide.

In Peptide C, a loss of the additional inflection points that occurred in peptide A was observed due to the elimination of His14 in the sequence (His14Cha mutation). The lack of inflection supported the hypothesis that His14 had to be present for proton transfer to occur. With the lack of histidine as the proton acceptor, the redox potential of Tyr5 increased (**Figure 1.10A**). Peptide E eliminated the hydrogen bond between Arg16 and Tyr5. Although a rather significant change in midpoint potential (~50 mV) was observed, there was no significant effect on the pK_a of His14 with the removal of the hydrogen bond (**Figure 1.10C**). The impact of π-cation interaction was studied using Peptide F. The interaction between Arg12 and Tyr5 was eliminated by mutation of the arginine to an isoleucine. A significant difference in midpoint potential was observed (again, ~50 mV), but the inflection points reflected those seen in Peptide A (**Figure 1.10D**). In the case of Peptide D, two mutations were made: Arg12Ala and His14Val. With His14 being mutated, inflection points accredited to that amino acid were not observed, and midpoint potential increases were observed at low and high pH values (**Figure 1.10B**).

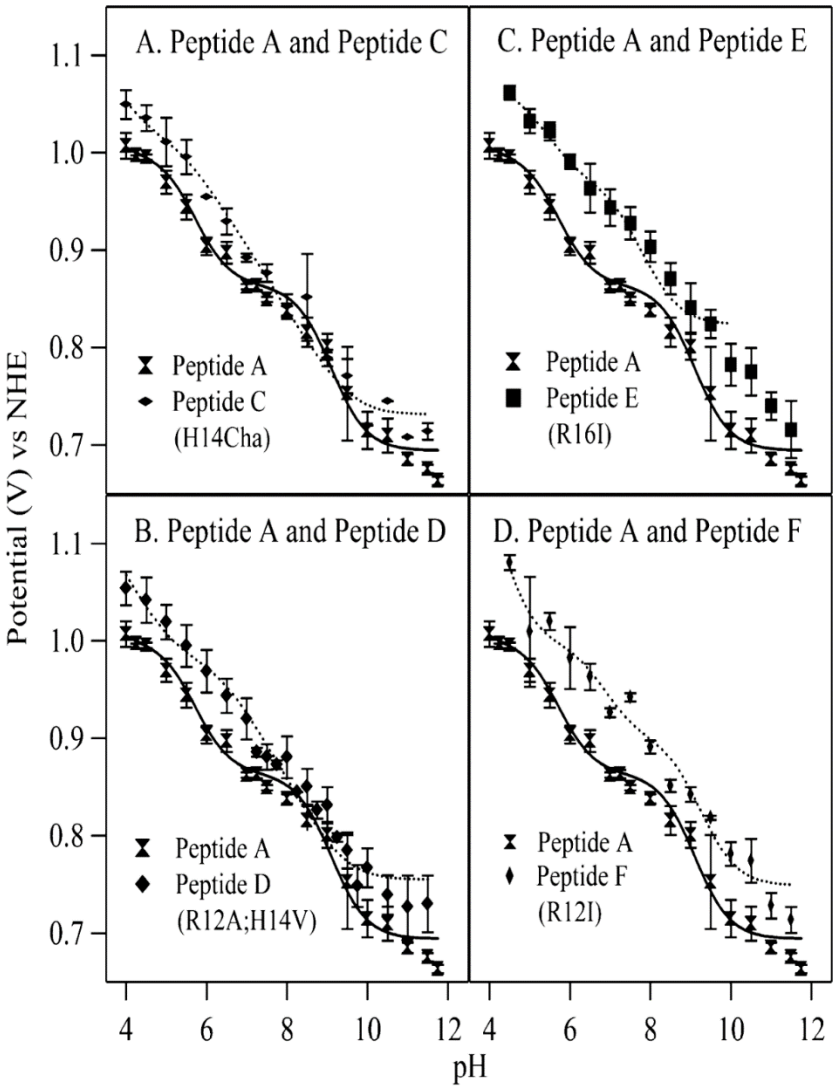

Figure 1.10. Electrochemical titrations of various peptides.[31]

The results discussed above for each peptide were fit to the Nernst equation to allow for multiple ionizable groups to possibly influence the potentials, and those values are reported in **Table 1.2**. The values of tyrosine oxidation were assigned to 0.0, and the various other oxidative species were assigned to the various peptides, as shown in the table. The values at pH 2.8 and 5.8 were consistent with a tyrosine-oxidation induced electrostatic perturbation of Asp3. The inflections at pH 6.0 and 9.0 were associated with the redox-induced changes in His14 in the forms

of the peptide where tyrosine is reduced and oxidized, respectively. Between the values of pH 6-9, a histidine PCET reaction likely occurred due to the protonation of His14 when Tyr5 is oxidized.[31]

Table 1.2. Parameters of Electrochemical Titration Data[31]

Sample	E (V)	Tyr^{red}	Asp^{ox}	Asp^{red}	His^{ox}	His^{red}
Tyrosine	1.35 ± 0.01	9.8 ± 0.1				
Peptide A	2.5 ± 0.2	9.3 ± 0.1	5.8 ± 0.6	2.8 ± 0.9	9.0 ± 0.1	6.0 ± 0.6
Peptide C (H14Cha)	1.33 ± 0.04	9.6 ± 0.1	5.6 ± 1.2	4.6 ± 1.0		
Peptide D (R12A; H14V)	1.6 ± 0.3	9.4 ± 0.3	7.3 ± 0.8	5.2 ± 0.5		
Peptide E (R16I)	2.5 ± 0.3	8.3 ± 0.1	5.6 ± 0.2	3.4 ± 0.2	7.9 ± 0.1	5.9 ± 0.2
Peptide F (R12I)	2.1 ± 0.1	9.6 ± 0.1	6.8 ± 0.6	4.5 ± 0.3	9.0 ± 0.1	7.3 ± 0.5

From these β-hairpin model studies, the group concluded that in Peptide A, PCET occurred between a cross strand histidine when a tyrosine was oxidized. Specifically, a proton was transferred to the histidine upon the oxidation of the tyrosine. The two amino acids were not directly hydrogen bonded but were able to interact through a bridging solvent. A decrease in potential occurred when tyrosine was hydrogen bonded or experienced a π-cation interaction, indicating the mechanisms of PCET were indeed altered with the changes. This work highlighted the impact of environmental interactions on the redox potentials of tyrosine, though the sidechain was exposed to solvent.

1.5.2 Artificial Triple Helix 'Protein'

A large portion of the work regarding the mechanism of electron transfer in polypeptide systems involving tyrosine and tryptophan has been done by a group led by Cecilia Tommos.[4] Their work builds upon that done by the Barry group discussed above and illustrates the impact of the driving force for PCET by secluding the sidechains from solvent using a larger, more structured environment than the β hairpin peptide by the Barry group.[26,31] They conclude that in proteins, side chain reductions typically occur at high potentials and involve single-electron exchanges via radical formation. To further probe the control of the redox potentials by the protein, the group created a mock-protein environment that consisted of 67 residues with a molecular mass of 7.4 kDa. The polypeptide was designed to fold into three alpha helices centered around an inner core which contained a single aromatic side chain, either tyrosine or tryptophan (at position 32). The single redox active amino acid meant that the only electrochemical signal would be produced by the aromatic amino acid. Protein characterization methods (such as CD and NMR) confirmed the presence of alpha helical structures and determined the proteins, α_3Y and α_3W, were thermodynamically stable in water with a resistance to changes in pH. Their tertiary structures were well defined, and the aromatic side chains were found to be fairly shielded from the bulk phase (**Figure 1.11**). The aromatic sidechain was designed to be excluded from the solvent environment to generate possible interplay between the protein environment and/or interactions and the radical. The de novo proteins were meant to reflect naturally occurring proteins that contained a buried redox-active amino acid.[32]

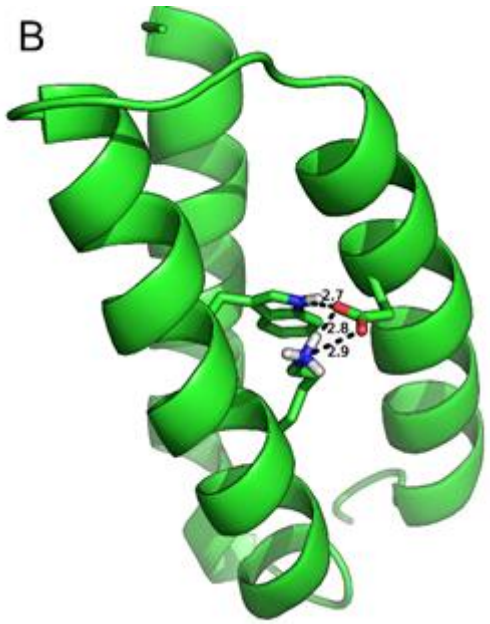

Figure 1.11. NMR derived structure of α_3W de novo protein.[4]

The protein which contained tyrosine in the center, α_3Y, was studied first. It is known that tyrosine can form three redox couples: Y-OH•+/Y-OH, Y-O•/Y-O-, Y-O•/Y-OH. The cation pair (Y-OH•+/Y-OH) is formed at pH below the pK_a of the oxidized state. The tyrosinate (Y-O•/Y-O-) is formed at pH above the pK_a of the reduced state, while the neutral tyrosine (Y-O•/Y-OH) exists between the two regions. It was predicted that Y-O•/Y-OH was the prominent redox pair that would be formed upon oxidation of the protein.

The group began by determining the electrochemical reversibility of the protein system. This was found by calculating the ratio of the forward current (I_{for}) to the reverse current (I_{rev}). A ratio of 1:1 corresponded to a reversible system. Anything higher or lower was irreversible. **Figure 1.12A-C** illustrated the currents for α_3Y at various frequencies to determine what frequency was required to create a reversible system. It was discovered that frequencies around 540 Hz and above probed a readily reversible reaction. However, the potentials (net, forward, and reverse) were not

independent of frequency until 750 Hz (**Figure 1.12D**). This autonomy was reflective of a fully reversible electrode system.[33,34] Furthermore, the current ratio declined from 30 Hz (1.71 ± 0.14) until it reached a limiting value between 750-960 Hz (1.01 ± 0.02) (**Figure 1.12E**). And although the forward and reverse potentials varied within the frequency range, the net potential only saw small changes (8 ± 2 mV between 30-120 Hz and 4 ± 2 mV between 120-960 Hz). In the higher range, the net potential reached 918 ± 2 mV vs NHE, the formal potential of the Y-O•/Y-OH redox couple (**Figure 1.12D**). The half-wave potentials were graphed versus pH as well (**Figure 1.12F**). The nonlinear relationship between pH 4.7-9.0. Upon closer inspection, the half-wave potential at pH 8.40 ± 0.01 was 916 ± 3 mV. Therefore, there was no significant difference between the half-wave and formal potentials of the Y-O•/Y-OH pair.

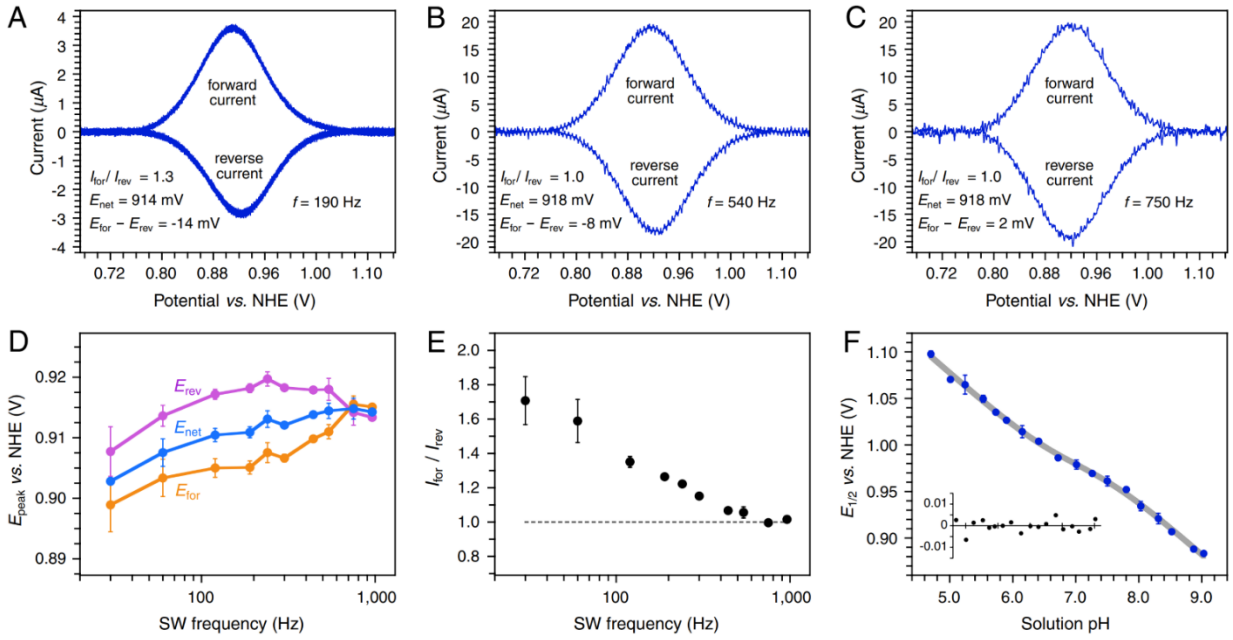

Figure 1.12. A-C. Forward and reverse currents for α_3Y (pH 8.40 ± 0.01) measured at various frequencies using SWV. D. The net potential (E_{net}), forward potential (E_{for}), and reverse potential (E_{rev}) as a function of frequency. E. The ratio of the peak of the forward and reverse current plots as a function of frequency. F. Half-wave potential ($E_{1/2}$) as a function of pH.[35]

The fact that Y32 was able to produce a fully reversible voltammogram supported the conclusion that the radical state was stable on the time scale of the oxidation/reduction reaction (≥ 30 ms). The well-structured environment surrounding the radical site aided in its stabilization by suppressing side reactions such as intermolecular radical-protein interactions.

The work was expanded toward tryptophan in the de novo protein. Tryptophan added another complex layer to the study as its structure is more complex and continue to discuss tryptophan being more complex and reference image of structure.[32] The potentials of α_3W were measured using SWV, and the first experiments determined the frequency dependence of the system. Tryptophan has two possible redox couples: N•/NH and NH•+/NH. It was found that there was no significant change in potential of the redox couple from 210-270 Hz at pH 9.9. From there, the pH dependence was studied. α_3W was prepared and analyzed at pH 9.9, pH 8.4, and pH 6.9, so at or around biological pH and higher. It was discovered that from pH 6.9 to pH 9.9, a potential difference of 55 ± 2 mV was obtained. Thus, the potentials of the protein were dependent upon the pH of the system (55 ± 2 mV/pH unit). This implied that approximately one proton was released upon oxidation of the W32, and the single proton was 'taken up' once radical reduction occurred. Overall, it was concluded that α_3W oxidized in a reversible manner (on a time scale of 3.5-4.8 ms), and the overall charge of the PCET process was neutral.

A Pourbaix diagram in **Figure 1.13** showed the pH dependency of α_3Y and α_3W. Both of showed regions of linear regression that denoted the pH values at which the proteins' potentials were controlled by the pH of the system. The red and blue regions of the diagram (tryptophan oxidation and tyrosine oxidation respectively) were produced by averaging the raw data sets gathered by the Group. The values at pH 7.0 shown were not actually measured but rather taken

from the line produced. A difference was observed between the Y32 and W32 pH-dependent regions. The tryptophan potentials were approximately 100 mV higher than the tyrosine potentials, indicating the tyrosine was more readily oxidizable.

The green and orange lines were produced using the pK_{ox} value of tryptophan and the pK_{red} value of tyrosine. They were not measured electrochemically. The pK_{ox} value of 3.4 was calculated by substituting phenylalanine (a redox inactive aromatic amino acid) in the place of Y32 within the α_3Y protein. Performing this substitute resulted in a pK_{red} change of 0.83 ± 0.06.[36] The Group predicted that a similar shift would be seen for the α_3W protein. It is also known that aqueous W has a pK_{ox} of (4.2-4.3) ± 0.1.[37,38] Thus, the pK_{ox} of α_3W was calculated as 4.25 - 0.83 = 3.4. The pK_{red} value of α_3Y was determined in previous work. From these values, the remainder of the pH-dependent region and the pH-independent region (where the graph plateaus) were predicted. The plateau regions were estimated by inputting the pK_{ox} and pK_{red} values that would generate a curve upon reaching said values that would then create a horizontal line.

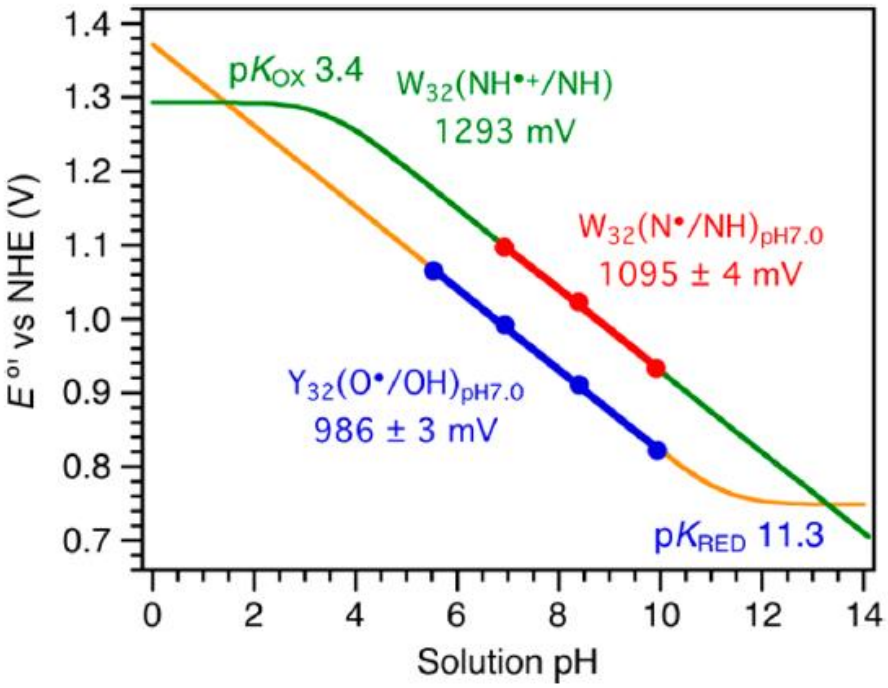

Figure 1.13. A Pourbaix diagram depicting the potentials of α_3Y and α_3W as a function of pH. The pK_{ox} and pK_{red} values were derived from solution titrations.[4]

Valuable information was gathered regarding the impact of a protein-like environment on the radical transfer of both tyrosine and tryptophan. The overall major impact of the surrounding environment was the stabilization of the radical which resulted in an extended lifetime. The stabilization was achieved by the protein matrix suppressing side reactions with solvent. When comparing the potentials (at pH 7.0) of the α_3Y and α_3W proteins to the potentials of aqueous Y and W, there were approximate differences of 45-65 mV and 65 mV, respectively.[36] The difference observed between the potentials of W32(N•+/NH) and W(N•+/NH) was around 100 mV. Similarly, the difference observed between W32(N•+/NH) and Y32(O•/OH) was approximately 100 mV. These results underscore the role of the protein in modulating the reduction potentials of tyrosine and tryptophan.

1.6 Thesis Summary

The initial goal of the thesis was to develop of method for direct electrochemical detection of potentials of tryptophan and tyrosine in a protein system. The work done by the Barry and Tommos groups was excellent and set the stage for the current work, but there were some knowledge gaps from their work and disadvantages to their systems. Perhaps the most obvious disadvantage was an absence of inquiry regarding the modulation of reduction potentials by a more complex protein environment. The two groups had addressed the manipulation of oxidation potentials in peptide and small, de novo environments, but there was a lack of information regarding what would occur in a natural, complex protein environment. The Barry group discovered great information regarding Y in a (poly)peptide system. They probed systems where π-cation interactions were present as well as systems where hydrophobic and aromatic interactions were occurring.[26,31] The limitation to this work, however, is that (poly)peptide systems are fully solvated whereas Y in a protein environment would be largely solvent excluded. The Tommos group solved the latter problem by sequestering the tyrosine sidechain into a de novo triple helix protein.[4,35] Although it was protein-like and provided deeper insight about how the protein can modulate amino acid radical redox potentials, the Group failed to manipulate electrostatics and discuss how to isolate possible overlapping electrochemical signals. Thus, the information discussed within this thesis is important because it addresses the question of how a protein's structural environment would impact the oxidation potentials of ET occurring through an amino acid within that protein's sequence.

For this thesis, we chose to assess the reduction potentials of tryptophan and tyrosine radicals within the model protein system, azurin. Azurin (Az) is a type 1 copper protein that has a

brilliant blue color in its wild-type (WT) form. It is a small (~14 kDa) protein that is involved primarily in bacterial anaerobic respiration. It is also mononuclear in its electron transfer process. Azurin was primarily chosen due to its size, structure, excellent thermal stability, and distinct spectroscopic characteristics; it can also be prepared recombinantly so it can be manipulated by site-directed mutagenesis. Importantly, it contains a single tryptophan. The latter is necessary to measure electrochemical potentials from a single redox cofactor.[39-41] There are a few other single tryptophan proteins that could have been used, such as RNase T1, nuclease, monellin, and glucagon. However, those proteins contain either tryptophan residues that are not buried (or solvent excluded) as gauged by their fluorescence emission spectra or too many tyrosine residues that complicate spectroscopic and electrochemical analysis.[42] Too many tyrosine and/or tryptophan residues would mean too many mutations necessary to single out the redox activity of a single amino acid. The multiple mutations could result in stability issues if the protein remained intact at all. The lack of a buried tryptophan would negate the purpose of the project: to study how a surrounding protein environment would impact the redox potentials. Therefore, azurin, with its single tryptophan residue and two tyrosine residues – mutated to phenylalanine - was the best option for a model system. To electrochemically probe the isolated redox potentials, SWV was used due to its higher sensitivity. CV was not sensitive enough to monitor oxidation and reduction in such a large system.

Chapter 2 details the characterization and study of two previously characterized azurin variants that contain tryptophan in different positions: W48 and W108 (W48 was mutated to phenylalanine and the tyrosine at 108 was mutated to tryptophan). These protein variants have been well characterized by CD, UV-visible, fluorescence, Raman (vibrational), and EPR spectroscopies. W48 is buried in a hydrophobic protein environment with no interactions with

solvent or a polar group. W108, conversely, is located near the surface of the protein and W108 is solvent accessible rather than solvent excluded. This tryptophan has the ability to hydrogen bond. In this chapter, SWV analysis determined a reduction potential difference of ~ 100 mV between W48 and W108, providing a proof-of-principle that the protein environment can control the potentials.

Chapter 3 is an extension of work presented in Chapter 2, with an important difference. In this chapter, we present newly engineered variants of azurin that compare reduction potentials of Y versus W. In both cases, the position of 48 was chosen as the position for the redox cofactor. For Y48, specific bases (including Asp and His) were introduced to assess the impact of H-bonding on the reduction potentials of Y. For W48, the cross-strand Phe110 was mutated to either small hydrophobic groups (Ala, Leu) or a polar sidechain (Ser) that introduce water molecules – determined by a combination of UV/vis, fluorescence and X-ray crystallography. SWV on these samples present new information into how local electrostatics can modulate the reduction potentials of amino acid radicals in proteins.

References

1. Sjulstok, E.; Olsen, J. M. H.; Solov'yov, I. A. Quantifying electron transfer reactions in biological systems: what interactions play the major role? *Scientific Reports* **2015**, *5*, 18446.
2. Sjoberg, B. M.; Reichard, P.; Graslund, A.; Ehrenberg, A. The Tyrosine Free Radical in Ribonucleotide Reductase from *Escherichia coli*. *J. Biol. Chem.* **1978**, *253*, 6863-6865.

3. Barry, B. A.; Chen, J.; Keogh, J.; Jenson, D.; Offenbacher, A.; Pagba, C. Proton Coupled Electron Transfer and Redox Active Tyrosines: Structure and Function of the Tyrosyl Radicals in Ribonucleotide Reductase and Photosystem II. *J. Phys. Chem. Lett.* **2012**, *4*, 543-554.
4. Glover, S. D.; Tyburski, R.; Liang, L.; Tommos, C.; Hammarström, L. Pourbaix Diagram, Proton-Coupled Electron Transfer, and Decay Kinetics of a Protein Tryptophan Radical: Comparing the Redox Properties of W32• and Y32• Generated Inside the Structurally Characterized α_3W and α_3Y Proteins. *J. Am. Chem. Soc.* **2018**, *140*, 185-192.
5. Osteryoung, J. G.; Osteryoung, R. A. Square Wave Voltammetry. *Analytical Chem.* **1985**, *57*, 101A-110A.
6. Mirceski, V.; Skrzypek, S.; Stojanov, L. Square-wave voltammetry. *ChemTexts* **2018**, *4*, 1-14.
7. Piccioli, M.; Luchinat, C.; Mizoguchi, T. J.; Ramirez, B. E.; Gray, H. B.; Richards, J. H., Paramagnetic NMR spectroscopy and coordination structure of cobalt(II) Cys112Asp azurin. *Inorg. Chem*. **1995**, *34*, 737-742.
8. Crespilho, F. N.; Zucolotto, V.; Oliveira Jr., O. N.; Nari, F. C. Electrochemistry of Layer-by-Layer Films: a review. *Int. J. Electrochem. Sci*. **2006**, *1*, 194-214.
9. Marcus, R. A. Chemical and Electrochemical Electron-Transfer Theory. *Annu. Rev. of Phys. Chem.* **1964**, *15*, 155-196.
10. Silverstein, T. P. Marcus Theory: Thermodynamics CAN Control the Kinetics of Electron Transfer Reactions. *J. Chem. Educ.* **2012**, *89*, 1159-1167.
11. Marcus Theory for Electron Transfer. (2020, December 12). Retrieved November 12, 2020, from https://chem.libretexts.org/@go/page/107311.

12. Nernst Equation. (2020, August 15). Retrieved November 12, 2020, from https://chem.libretexts.org/@go/page/273.
13. Electrochemistry Basics. (2020, August 15). Retrieved April 9, 2021, from https://chem.libretexts.org/@go/page/251.
14. Gamry Instruments. Two-, Three-, and Four-Electrode Experiments. In *Application Note*, Rev. 3.0; 2015. Two,Three,Four Electrode System Gamry 4-Probe Potentiostats
15. Elgrishi, N.; Rountree, K. J.; McCarthy, B. D.; Rountree, E. S.; Eisenhart, T. T.; Dempsey, J. L. A Practical Beginner's Guide to Cyclic Voltammetry. *J. Chem. Educ.* **2018**, *9*, 197-206.
16. Khan, M. S.; Asif, A.; Khawaldeh, S.; Tekin, A. Dopamine Detecting using Mercaptopropionic Acid and Cysteamine for Electrodes Surface Modification. *J. Electr. Bioimpedance* **2018,** *1*, 83.
17. El-Hady, D. A.; Abdel-Hamid, M. I.; Seliem, M. M.; Andrisano, V.; El-Maali, N. A. Osteryoung square wave stripping voltammetry at mercury film electrode for monitoring ultra trace levels of Tarabine PFS and its interaction with ssDNA. *J. Pharm. Biomed. Anal.* **2004,** *5*, 879-890.
18. Gulaboski, R.; Lovric, M.; Mirceski, V.; Bogeski, I.; Hoth, M. Protein-film voltammetry: A theoretical study of the temperature effect using square-wave voltammetry. *Biophysical Chemistry* **2008**, *137*, 49-55.
19. Armstrong, F. A. Insights from protein film voltammetry into mechanisms of complex biological electron-transfer reactions. *J. Chem. Soc., Dalton Trans.* **2002,** *5*, 661-671.

20. Robb, A. J.; Vinogradov, S.; Danell, A. S.; Anderson, E.; Blackledge, M. S.; Melander, C.; Hvastkovs, E. G. Electrochemical Detection of Small Molecule Induced Pseudomonas aeruginosa Biofilm Dispersion. *Electrochimica Acta* **2018**, *1*, 276-282.
21. Barry, B. A.; Einarsdottir, O. Insights into the structure and function of redox-active tyrosines from model compounds. *J. Phys. Chem. B* **2005**, *109*, 6972-6981.
22. Britt, R. D. In Oxygen Photosynthesis: The Light Reactions; Ort, D. R., Yocum, C. F., Eds.; Cluwer Academic Publisher: Dordrecht, 1996; Vol. 4, pp 137-164.
23. Malkowski, M. G. G., S. L.; Smith, W. L.; Garavito, R. M. The productive conformation of arachidonic acid bound to prostaglandin synthase. *Science* **2000**, *289*, 1933-1937.
24. Stubbe, J.; van Der Donk, W. A. Protein Radicals in Enzyme Catalysis. *Chem. Rev.* **1998**, *98*, 705-762.
25. Whittaker, M. M.; Whittaker, J. W. A tyrosine-derived free radical in apogalactose oxidase. *J. Biol. Chem.* **1990**, *265*, 9610-9613.
26. Sibert, R.; Josowicz, M.; Poorcelli, F.; Veglia, G.; Range, K.; Barry, B. A. Proton-Coupled Electron Transfer in a Biomimetic Peptide as a Model of Enzyme Regulatory Mechanisms. *J. Am. Chem. Soc.* **2007,** *129*, 4393-4400.
27. Dixon, W. T.; Murphy, D. Determination of the acidity constants of some phenol radical cations by means of electron spin resonance. *J. Chem. Soc., Faraday Trans. 2* **1976**, *72*, 1221- 1229.
28. Rhile, I. J.; Markle, T. F.; Nagao, H.; DiPasquale, A. G.; Lam, O. P.; Lockwood, M. A.; Rotter, K.; Mayer, J. M. Concerted Proton-Electron Transfer in the Oxidation of Hydrogen-Bonded Phenols. *J. Am. Chem. Soc*. **2006**, *128*, 6075-6088.

29. Marcus, R. A. Electron transfer reactions in chemistry theory and experiment. *Pure Appl. Chem*. **1997**, *69*, 13-29.

30. Midpoint Potential. Oxford Reference. https://www.oxfordreference.com/view/10.1093/oi/authority.20110803100156634#:~:text=Quick%20Reference,and%20the%20oxidant%20are%20equal (accessed Dec 01, 2020). x Moore, G. R.; Pettigrew, G. W. Cytochromes c. Evolutionary, Structural, and Physiochemical Aspects; Springer-Verlag: Berlin, 1990.

31. Sibert, R. S.; Josowicz, M.; Barry, B. A. Control of Proton and Electron Transfer in *de Novo* Designed, Biomimetic β Hairpins. *ACS Chem. Biol.* **2010,** *5*, 1157-1168.

32. Tommos, C.; Skalicky, J. J.; Pilloud, D. L.; Wand, A. J.; Dutton, P. L. De Novo Proteins as Models of Radical Enzymes. *Biochemistry* **1999**, *38*, 9495-9507.

33. Osteryoung, J. and O'Dea J. J. Square-Wave Voltammetry. In Electroanalytical Chemistry, ed AJ Bard; Marcel Dekker: New York, 1986; Vol 5, pp 209-308.

34. Mirceski, V.; Komorsky-Lovric, S.; Lovric, M. Square-Wave Voltammetry: Theory and Applications. In Monographs in Electrochemistry, ed F Scholz; Springer-Verlag: Berlin, 2007.

35. Berry, B. W.; Martinez-Rivera, M. C.; Tommos, C. Reversible voltammograms and a Pourbaix diagram for a protein tyrosine radical. *PNAS* **2012**, *109*, 9739-9743.

36. Ravichandran, K. R.; Zong, A. B.; Taguchi, A. T.; Nocera, D. G.; Stubbe, J.; Tommos, C. Formal Reduction Potentials of Difluorotyrosine and Trifluorotyrosine Protein Residues: Defining the Thermodynamics of Multistep Radical Transfer. *J. Am. Chem. Soc*. **2017**, *139*, 2994-3004.

37. (a) Posener, M. L.; Adams, G. E.; Wardman, P.; Cundall, R. B. Mechanism of tryptophan oxidation by some inorganic radical-anions: a pulse radiolysis study. *J. Phys. Chem. Soc., Faraday Trans. 1* **1976**, *72*, 2231-2239. (b) Baugher, J. F.; Grossweiner, L. I. Photolysis mechanism of aqueous tryptophan. *J. Phys. Chem.* **1977**, *81*, 1349-1354.

38. Solar, S.; Getoff, N.; Surdhar, P. S.; Armstrong, D. A.; Singh, A. Oxidation of Tryptophan and N-Methylindole by N3\ Br2*", and (SCN)2- Radicals In Light and Heavy-Water Solutions: A Pulse Radiolysis Study. *J. Phys. Chem.* **1991**, *95*, 3639-3643.

39. Nar, H.; Huber, R.; Messerschmidt, A.; Filippou, A. C.; Barth, M.; Jaquinod, M.; van de Kamp, M.; Canters, G. W. Characterization and crystal structure of zinc azurin, a by-product of heterologous expression in *Escherichia coli* of *Pseudomonas aeruginosa* copper azurin. *European Journal of Biochemistry* **1992**, *205*, 1123-1129.

40. Romero, A.; Hoitink, C. W. G.; Nar, H.; Huber, R.; Messerschmidt, A.; Canters, G. W. X-ray Analysis and Spectroscopic Characterization of M121Q Azurin: A Copper Site Model for Stellacyanin. *J. Mol. Bio.* **1993,** *229*, 1007-1021.

41. Marshall, N. M.; Garner, D. K.; Wilson, T. D.; Gao, Y.-G.; Robinson, H.; Nilges, M. J. Lu, Y. Rationally tuning the reduction potential of a single cupredoxin beyond the natural range. *Nature* **2009**, *462*, 113-116.

42. Lakowicz, J. R. Protein Fluorescence. In *Principles of Fluorescence Spectroscopy,* 3rd ed; Springer, 2006. Protein Fluorescence | SpringerLink

CHAPTER 2

Impact of Local Electrostatics on the Redox Properties of Tryptophan Radicals in Azurin: Implications for Redox-Active Tryptophans in Proton-Coupled Electron Transfer

Kristin J. Tyson, Amanda N. Davis, Jessica L. Norris, Libero J. Bartolotti, Eli G. Hvastkovs, and Adam R. Offenbacher

Reproduced with permission from *The Journal of Physical Chemistry Letters*

Abstract. Tyrosine and tryptophan play critical roles in facilitating proton-coupled electron transfer (PCET) processes essential to life. The local protein environment is anticipated to modulate the thermodynamics of amino acid radicals to achieve controlled, unidirectional PCET. Herein, square-wave voltammetry was employed to investigate the electrostatic effects on the redox properties of tryptophan in two variants of the protein azurin. Each variant contains a single redox-active tryptophan, W48 and W108, in a unique and buried protein environment. These tryptophan residues exhibit reversible square-wave voltammograms. A Pourbaix plot, representing the reduction potentials versus pH, is presented for the non-H-bonded W48, which has comparable potentials with tryptophan in solution. The reduction potentials of W108 are seen to be increased by more than 100 mV across the same pH range. Molecular dynamics show that, despite its buried indole ring, the N-H of W108 hydrogen bonds with a water cluster, while W48 is completely excluded from interactions with water or polar groups. These redox properties provide insight into the role of the protein in tuning the reactivity of tryptophan radicals, a requisite for controlled biological PCET.

Proteins exert exquisite directional control of long-range electron transfer through the fine tuning of donor-acceptor distances and local reaction driving forces.[1-5] These reactions are often mediated by the redox-active amino acids, tyrosine and tryptophan, in which sidechain oxidation is thermodynamically coupled to deprotonation through a proton-coupled electron transfer (PCET) process to form neutral radical species (**Figure 2.1**) potentials of these amino acid radicals are expected to be ~ 1 V, providing some of the highest oxidative power in biology. These high-potential redox cofactors are involved in numerous chemical transformations. For example, tryptophan radicals (W•), generated by PCET, have been shown to play key roles in DNA biosynthesis[1, 6] and repair,[7-8] lignin degradation,[9] and cellular respiration.[10-11] These 'hot' oxidants have also been implicated in providing off-pathway radical shunts to mitigate aberrant oxidative reactions in oxidoreductases.[12]

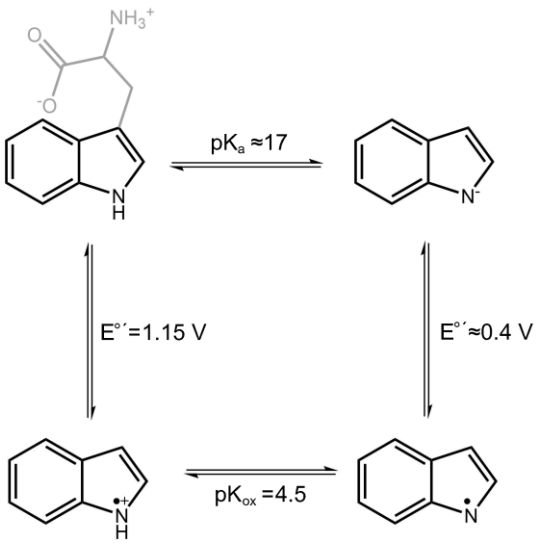

Figure 2.1. Thermodynamic cycle for tryptophan oxidation. For clarity, the backbone is shown in light gray for ground state tryptophan in upper left only. Potentials are versus NHE.

While many enzymes use the high potentials of tryptophan radicals in long-range electron transfer, little is known on how, for a defined and complex enzymatic system, their redox

properties are modulated to regulate the reactivity and directionality of the local PCET reactions. Reduction potentials of tyrosine and tryptophan radicals in complex proteins have been largely inferred from modeling charge transfer rates using modified Marcus-like formalisms (for examples, see refs [13-15]). A few reports on the direct electrochemical detection of tyrosine and tryptophan redox properties have emerged from the studies of small, biomimetic and artificial (poly)peptides;[16-18] however, the impact of distinct protein microenvironments on the thermodynamics of amino acid redox centers has hitherto been unresolved. To begin to address how the local electrostatics of a protein scaffold may influence these properties, we present an electrochemical study on two variants of the model protein azurin, each containing a single tryptophan sidechain with different solvent polarity and hydrogen bonding. This study provides important fundamental insight into the role of electrostatics in tuning the redox properties of tryptophan sidechains in proteins and in regulating long-range PCET linked to biological catalysis.

Azurin has served as a robust model protein for studying amino acid mediated electron transfer.[3, 19-21] *P. aeruginosa* azurin contains a single tryptophan residue at position 48 (native site) and two tyrosine sidechains (Y72 and Y108). For the purpose of this study, a tyrosine-deficient azurin variant,[22] which is referred to as azurin W48 (W48/Y72F/Y108F), was utilized to enable direct electrochemical detection of tryptophan redox properties. Structural and spectroscopic studies have been employed to characterize both the singlet and the (photolysis-generated) radical states of the tryptophan at position 48, leading to a consensus that W48 is buried in a low dielectric microenvironment.[22-25] For instance, the fluorescence spectrum of W48 exhibits both fine structure and the greatest blue-shifted emission wavelength (λ_{max} = 308 nm) for a tryptophan in a natural protein.[26-27] Such emission properties of W48 are unique for tryptophan residues in proteins and can only be modeled by indoles in non-polar solvents. In addition to W48, engineered azurin

variants have been reported in which the tryptophan residue is repositioned in regions with variable solvent exposure and hydrogen bonding.[21, 28] Azurin therefore provides an incisive system to examine the role of the protein milieu on the redox properties of amino acids. While many electrochemical studies have been centered on the $Cu^{2+/+}$ redox couple of azurin (for examples, see refs [29-32] and **Figure 2.2**), to our knowledge, the current work presents the first direct electrochemical measurements of the redox potentials of tryptophan sidechains in azurin.

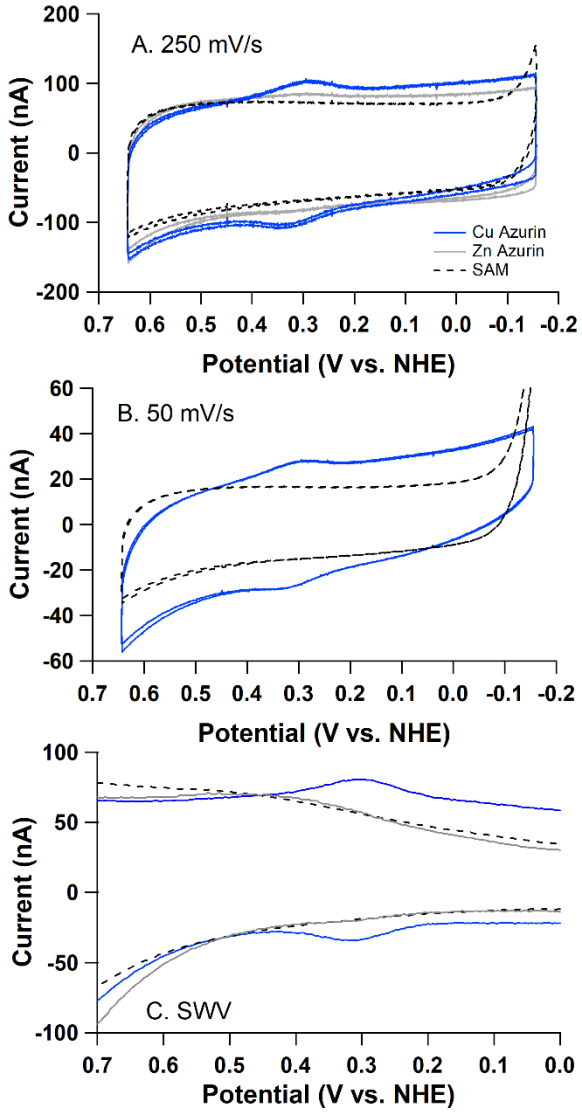

Figure 2.2. Azurin Cu(II/I) redox couple determined by representative CV (A and B) and SWV (C) measurements. The traces represent: solid blue, Cu-azurin; solid gray, Zn-azurin; and dashed line, SAM only (no protein). Azurin was immobilized on alkanethiol (1:1 6-mercapto-1-hexanol:1-hexanthiol) SAM-modified gold electrodes, as adapted from ref [33]. Solutions (5 μM in ethanol) of the alkanethiol mixture were applied to electrochemically cleaned Au electrode surface for 1 hour. The electrodes were rinsed and the protein sample (2 mg/mL) was applied to the surface (20 hours, 4°C). The buffer used for these experiments was 10 mM APB, pH 7.0. The potentials of Cu(II/I) couple determined from these experiments were 309-315 mV vs. NHE, within the reported range (see refs [29, 32], for examples).

Recombinant azurin, isolated from bacterial cultures, contains both Cu^{2+} and Zn^{2+}. For enhanced electrochemical responses, the metal was substituted for Zn^{2+} using standard protocols involving dialysis with cyanide solution (see Methods for details and **Figure 2.3**). Due to muted electrochemical responses generated from buried amino acids, pulsed differential or stepped potential methods, such as square-wave voltammetry (SWV), are often employed.[17, 34-35] Here, SWV was performed on films of azurin W48 (see **Methods** for details), producing a single peak at 952 ± 6 mV vs NHE at pH 7 (**Figure 2.4A**). This value is slightly lower than the potential for tryptophan in aqueous solutions recorded at the same pH (988 ± 5 mV; **Table 2.1**).[36-37] At f = 30 Hz, the intensities of the forward and reverse currents (I_{for} and I_{rev}) are approximately the same (**Figure 2.5A**), both supporting that the electrochemical response is reversible and permitting conversion of the peak potential, E_{net}, to $E°'$.[16, 35] The dependence of the electrochemical signal of W48 on the frequency parameter, f, of SWV was examined from 15 to 200 Hz (**Figure 2.5B**). While the signal intensity was sensitive to f, there were little-to-no significant differences seen for the magnitude of E_{net} (within 20 mV variation).

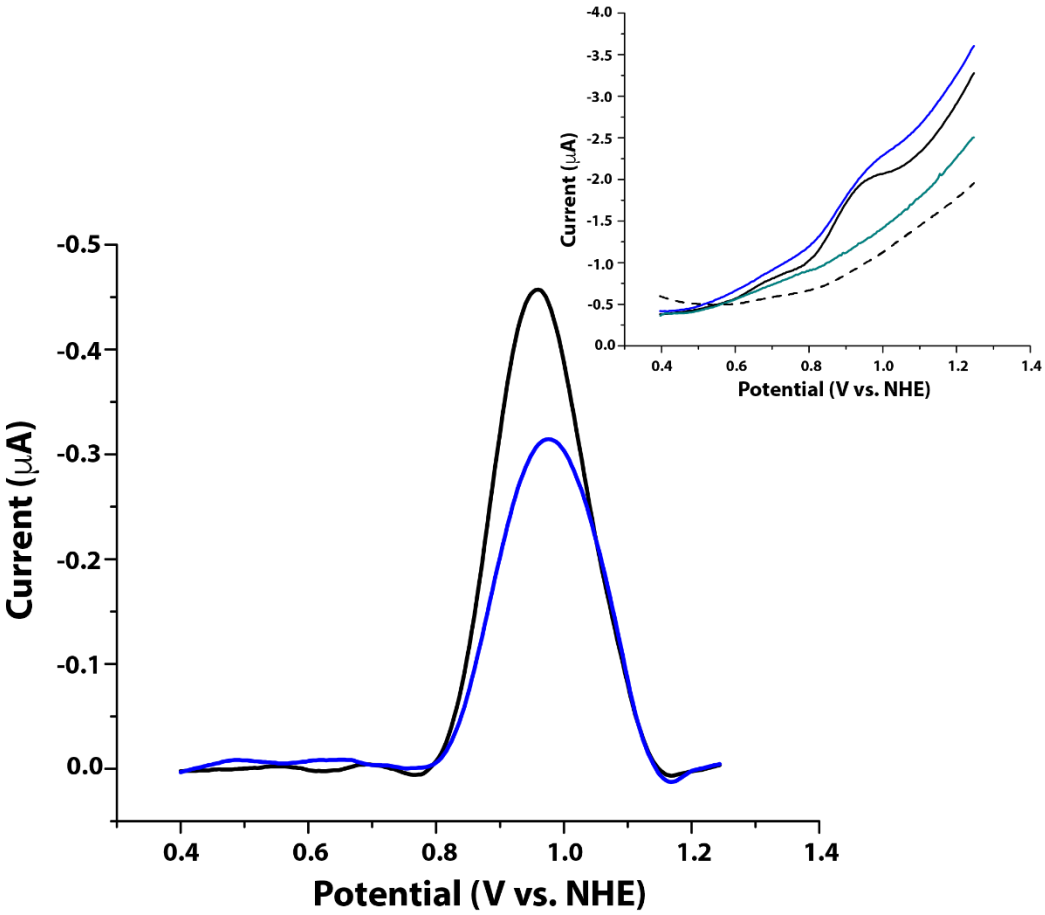

Figure 2.3. Background-subtracted SWV response for Zn^{2+}-substituted (black solid line) and as-isolated (denoted 'Cu^{2+}'; blue solid line) form of W48. The peak potentials are within 15 mV (vs NHE). *Inset*: Raw SWV traces prior to background subtraction. For reference, the responses from W48F (dotted black line) and the polymer alone (no azurin; green solid line) are shown.

Table 2.1. Electrochemical potentials for select protein tryptophan residues and their local environmental properties.

Variant	E_{net} (mV), pH 7	pK_{ox}	SASA (Å^2)	H-bonded?
AzW48	952 ± 6	≤ 3[a]	0[b]	No
AzW108	1070 ± 8	4.3 ± 0.3[a]	13.9 (7%)[c] 16.1 (9%)[d]	Yes
α_3W	1095 ± 4	3.4[e]	11.6 (6%)[f] 3.5 (2%)[g]	Yes
W (aq)[h]	988 ± 5	4.2 ± 0.2	188.0[i]	----

[a]Given the accessible pH range for E_{net} of W48 and W108, these values are estimates from representative fits to the Nernst equation. [b]Determined from the X-ray structure (PDB: 1E67). [c]Determined from X-ray structure (PDB: 1R1C). [d]Average value from 100 ns MD simulations presented here. [e]Extrapolated from a limited three-point pH study (pH 7–10); no uncertainty reported.[17] [f]Determined from NMR structures (PDB: 1LQ7). [g]Average value from 30 ns MD simulations presented here. [h]From the fit to the data presented in **Figure 2.6**. [i]Molecular solvent accessible area.

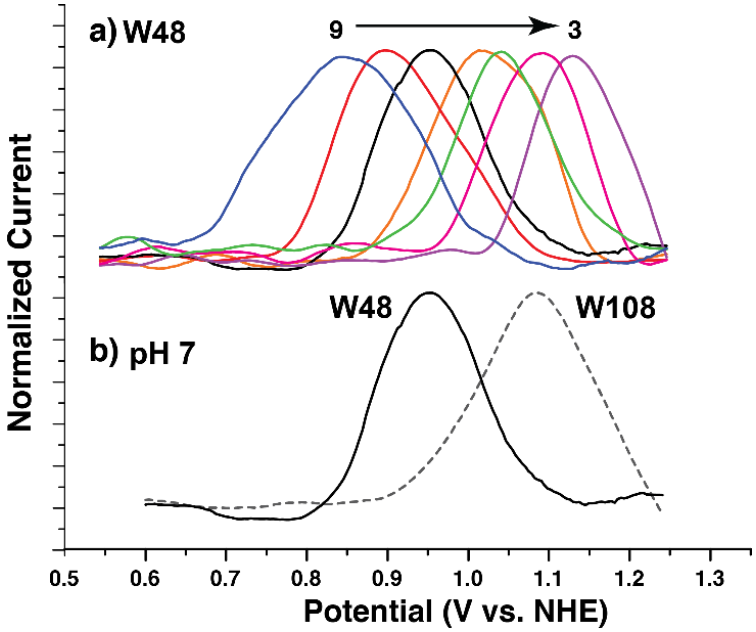

Figure 2.4. Background-subtracted SW voltammograms of azurin W48 as a function of pH, from 9 (blue trace) to 3 (purple trace) (A). Reversible, background-subtracted SW voltammograms for W48 (solid line) and W108 (dotted line), recorded at pH 7 (B). The pH dependent voltammograms (pH 3–9) of W108 are shown, for reference in **Figure 2.7**. SWV parameters were 30 Hz frequency and 10 μA sensitivity.

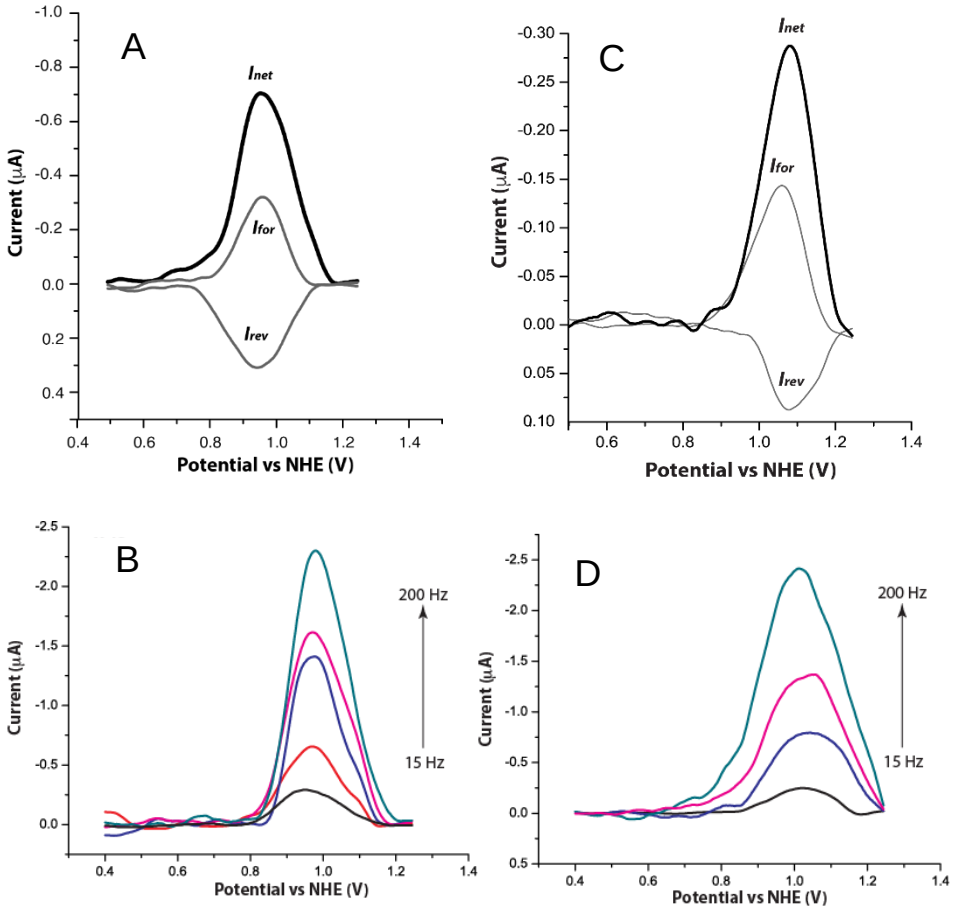

Figure 2.5. Background-subtracted SWV of (A) W48 and (C) W108 at f = 30 Hz, showing the forward (I_{for}) and reverse (I_{rev}) voltammograms. In (B) and (D), the net current, I_{net}, is presented for (B) W48 and (D) W108 as a function of *f:* black, 15 Hz; red, 30 Hz; blue, 50 Hz; fuchsia, 100 Hz; and cyan, 200 Hz. Note: there is slight variation (≤ 30 mV) in the peak potential as a function of SW frequency, *f*, for W108. Similar variation has been reported before in the case of tyrosine and tryptophan reduction potentials in the α_3Y and α_3W artificial protein systems.[16-17, 34] Further, this variation is comparable to the reproducibility (uncertainty) of electrochemical responses at a given frequency, acquired from triplicate/quadruplicate experiments (±6 to ±9 mV) and, importantly, it is significantly less than the differences in electrochemical responses between W108 and W48 at a given pH (> 100 mV; see **Figure 2.8**).

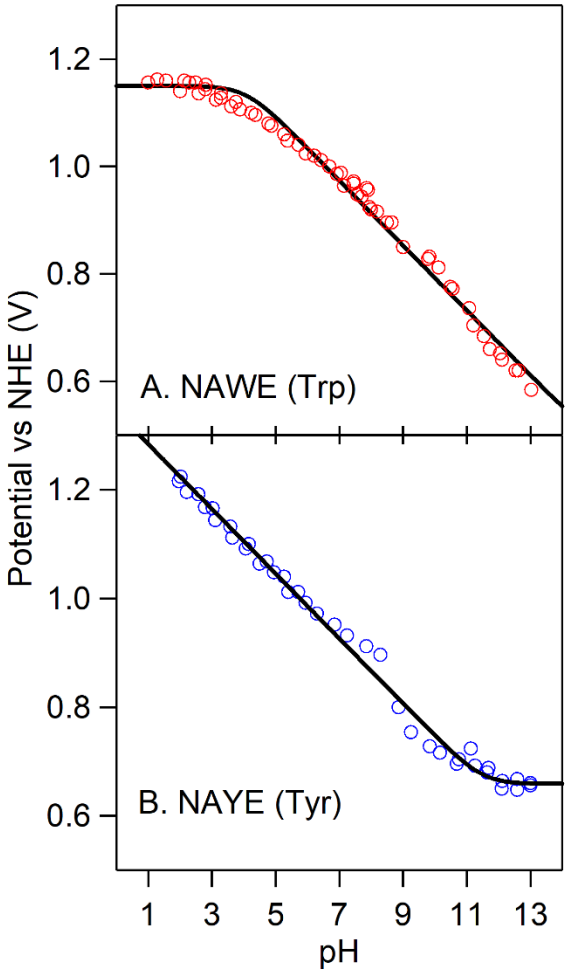

Figure 2.6. SWV data for NAYE and NAWE. Parameters are listed in **Figure 2.4**. The slopes of pH-dependent regions are (A) 0.061 ± 0.002 and (B) 0.060 ± 0.001 mV/pH. These are comparable to expectations from literature.[36, 38]

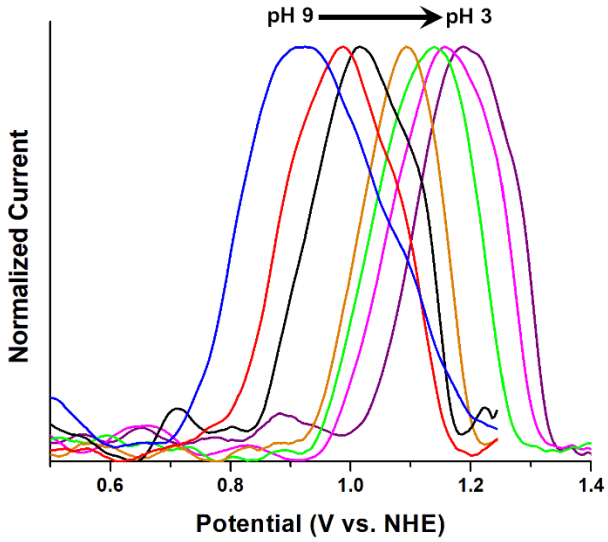

Figure 2.7. Background-subtracted SW voltammograms of azurin W108 as a function of pH. The SWV scanning parameters were frequency, 30 Hz and sensitivity, 1×10^{-5} A.

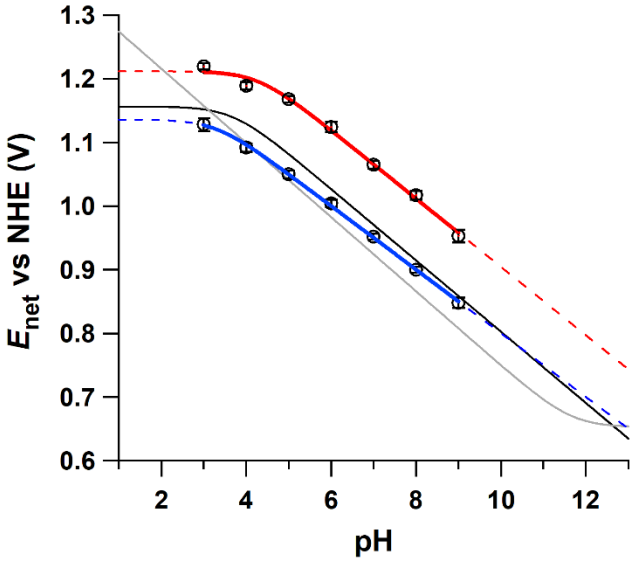

Figure 2.8. Pourbaix plots of W48 (blue) and W108 (red) potentials from **Figure 2.4** and **2.7**, respectively, compared to N-acetylated, esterified tyrosine, NAYE (thin gray line) and tryptophan, NAWE (thin black line). The error bars represent ± s.d. from 3-4 measurements. The raw data of NAYE and NAWE are presented in **Figure 2.6**. The slopes of the representative fits to the Nernst equation for W48 and W108 signify 49 (blue) and 53 (red) mV per pH, respectively.

We next sought to assign this electrochemical response to tryptophan through the mutation of the tryptophan at position W48 to phenylalanine (i.e. W48F). CD spectroscopy was used to show that this mutation maintains the characteristic β-sheet secondary structure of azurin (**Figure 2.9**). Further, its thermal stability (T_m = 73.5±0.7°C), derived from CD melts, is comparable to W48 (T_m = 74.0 ± 0.7).[39] The SW voltammogram seen for W48 in **Figure 2.4A** is lost in the case of W48F (**Figure 2.3**), confirming that the Faradaic response of azurin W48 originates from tryptophan. The electrochemical potential of W48 was then measured across a broad pH range of 3 to 9 (**Figure 2.4A**). The potential of W48 follows Nernstian behavior, decreasing 49±2 mV for each increase in pH unit, consistent with a PCET event (**Figure 2.8**, blue dots). The slight deviation from the theoretical slope of 59 mV per pH may be a consequence of a pH-induced change in the global protein electrostatics that influences the potential directly or circuitously through changes in protein structure.[17] A modified azurin, W108, has been reported, in which the native tryptophan at position 48 was mutated to phenylalanine and a tyrosine at position 108 was mutated to a tryptophan (W48F/Y72F/Y108W).[28] From its X-ray structure (PDB: 1R1C), the indole ring of W108 is anticipated to be buried but located proximal to the solvent interface. Using SWV as outlined above, the potential of W108 was determined to be 1070 ± 8 mV at pH 7, more than 100 mV higher than W48 under the same conditions (**Figure 2.4B**). The electrochemical response of W108 is reversible and is not significantly dependent upon the SWV frequency from 15-200 Hz (**Figure 2.2C, D**). The shifted potential of W108 also tracks across the pH range of 3 to 9 (**Figure 2.8**, red dots).

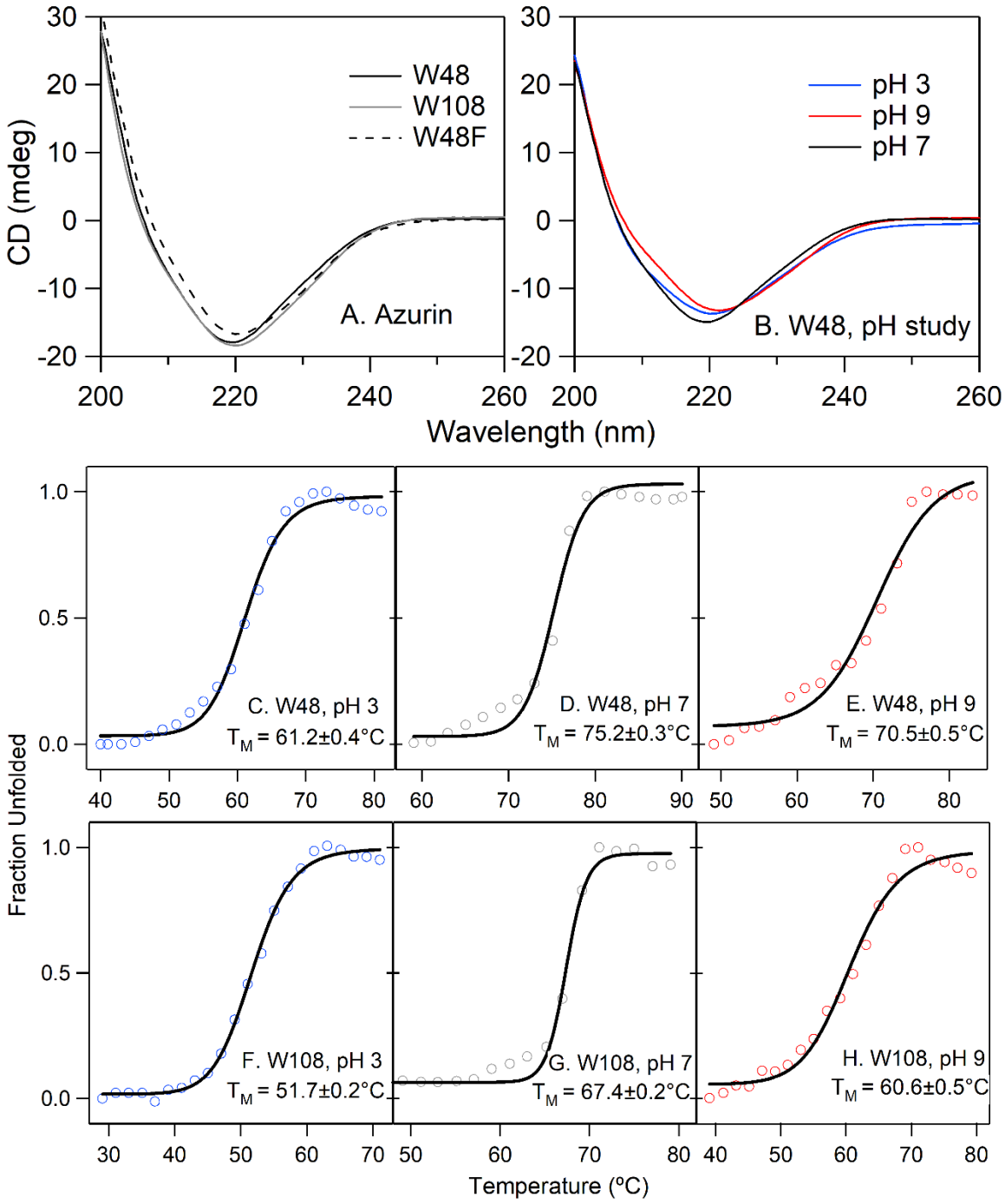

Figure 2.9. CD spectra of W48, W48F, W108 (A) and W48 as a function of pH (B). Representative plots of fraction unfolded vs temperature, determined by change in CD signal at 220 nm, presented in (C-H). The open circles are raw data while the black lines represent the fits to the data with the corresponding melting temperature (T_m) in the appropriate panel.

From the fitting of these data to the Nernst equation, the pK_{ox} of W108 was estimated as 4.3 ± 0.3, comparable to that of the tryptophan cation radical in solution (**Table 2.1**). Within the accessible pH range for structurally intact azurin, the electrochemical potentials of W48 do not greatly deviate from the 49 mV per pH dependence, implicating an altered acidity constant for the indoxyl radical. We therefore assign the pK_{ox} for W48 to be ≤ 3. The latter value is not surprising given the low dielectric nature of the environment surrounding W48[27] in which charge build-up would be thermodynamically unfavorable. However, instability of azurin at pH < 3 precludes an accurate assessment of this redox property. While there is uncertainty in the values of pK_{ox} for W48 and W108, the compelling result from this study is the significant difference in their reduction potentials that is maintained over a wide pH range.

The observation of an elevated reduction potential for W108, relative to model tryptophan, is consistent with a previous electrochemical study centered on a single tryptophan positioned in an artificial, triple helix bundle, α_3W. The α_3W exhibited a potential 1095 ± 4 at pH 7 (**Table 2.1**).[17] It had been rationalized the elevated potential of the tryptophan in α_3W is attributed to its sequestration from solvent. To explore this postulation further in the context of the results presented herein, we examined the X-ray structures of azurin (**Figure 2.10A**).[28, 40] W48 is completely solvent excluded and buried in a hydrophobic core, while W108 is closer to the surface. The only residue or atoms within 3.5 Å of the ring of W48 is F110; the two residues are arranged in a staggered π-π stacking orientation (**Figure 2.10B**). There are no other electrostatic interactions apparent. From the 1.9 Å X-ray structure of W108, solvent-accessible surface area (SASA) analysis, performed herein, shows that an estimated 7% of the tryptophan residue at position 108 is exposed to solvent (**Table 2.1**), compared to 0% for W48. To account for any changes in solvent

exposure from dynamic contributions of the protein matrix, we carried out 100 ns molecular dynamics (MD) simulations on solvated azurin (see **Methods** for details). The resulting model, generated from cluster analysis along the course of the 100 ns MD trajectory, shows a hydrogen bond between N-H from the W108 ring with a water molecule from a water cluster (**Figure 2.10C**). Apart from this, W108 is surrounded by aliphatic residues. Over the course of the MD simulation, the average RMSD (*ca.* 1 Å) values of the backbone atoms indicate the MD model is quite comparable to its crystal structure (**Figure 2.10**). Conversely, MD simulations carried out for azurin W48 showed that no water molecules penetrate the hydrophobic core of the protein (**Figure 2.11**). This structural analysis implicates that the increased electrochemical potential for W108, relative to W48, is likely attributed to a distinctive electrostatic interaction (i.e. hydrogen bonding with a water molecule) while the W108 ring is otherwise surrounded by a predominantly aliphatic pocket. The trend in the reduction potentials for W48 and W108 (**Table 2.1**) is further supported by the strength of their N-H stretch, measured by resonance Raman spectroscopy.[23] For example, the ω17 is an N-H bend mode sensitive to H-bonding.[41] W48 exhibits a lower frequency, relative to W108, for the ω17 vibrational mode, which supports a weaker N-H bond and, thus, is consistent with the lower reduction potential presented here.

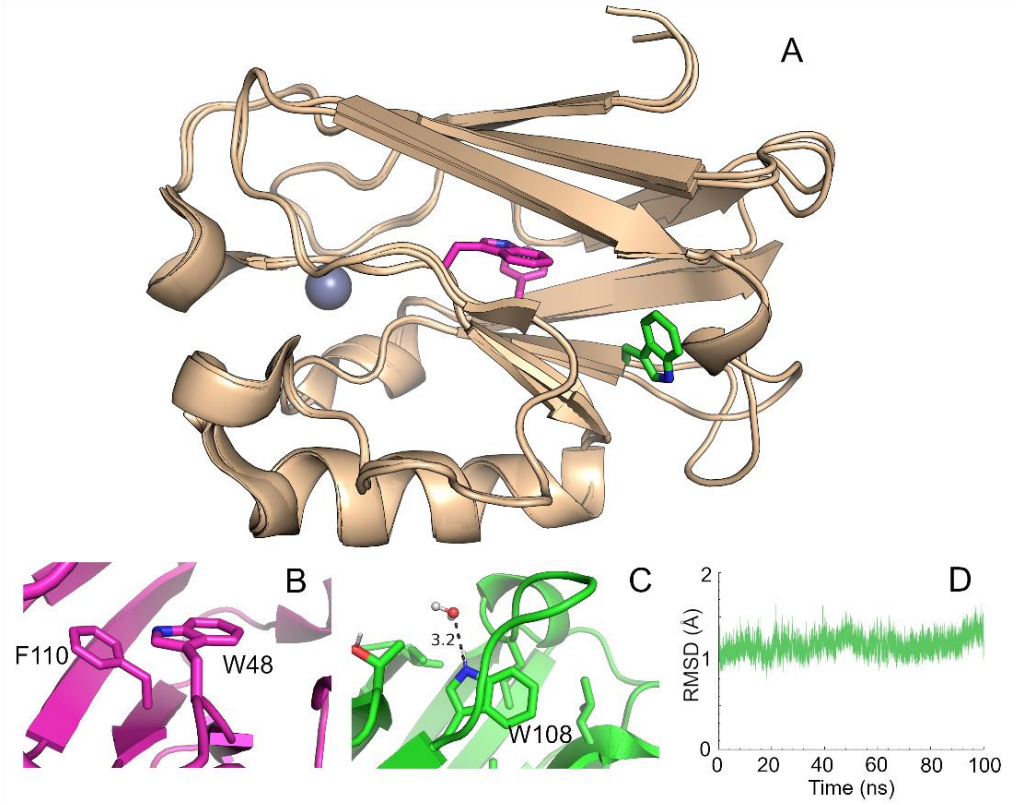

Figure 2.10. Overlaid X-ray structures of azurin W48 (magenta) and W108 (green) are presented in (A). The metal center is represented by a gray sphere. (B) is a zoomed-in view of W48, while (C) representative structure from cluster analysis of 100 ns MD simulation (see **Methods** for details). Residues or waters within 3.5 Å of the indole rings are also presented as sticks. (D) shows the average RMSD of W108.

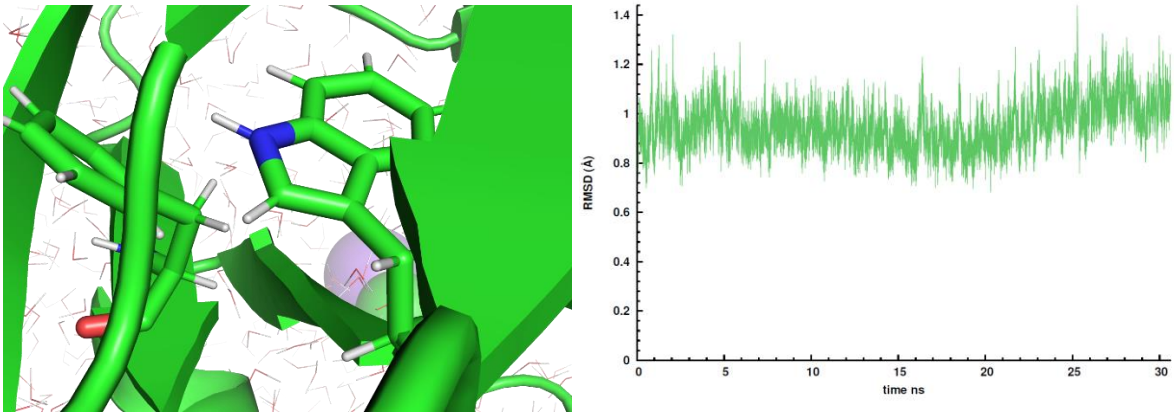

Figure 2.11. 30 ns MD model of W48 (left). The solvation shell is shown for reference; no water molecule penetrates the β barrel. *Right*: The RMSD along the 30 ns simulation.

From the NMR-determined α_3W structure (PDB: 1LQ7), 3.5-11.6 Å^2 or 2-6% of the indole ring is solvent exposed, with the N-H closest to solvent interface.[42] Using this NMR structure, we present a model from cluster analysis of a 30 ns MD simulation of α_3W (**Figure 2.12**). Despite being sequestered from solvent (i.e. 2-6% SASA), the tryptophan in α_3W also adopts hydrogen bonds but with polar sidechains rather than water. Therefore, we propose that the elevated potentials of α_3W, compared to tryptophan in solution, are not merely due to solvent exclusion,[17] but likely originate from an electrostatic field effect.[43] Similar increased potentials were predicted for an indole ring with a cation interaction in a low dielectric medium.[42]

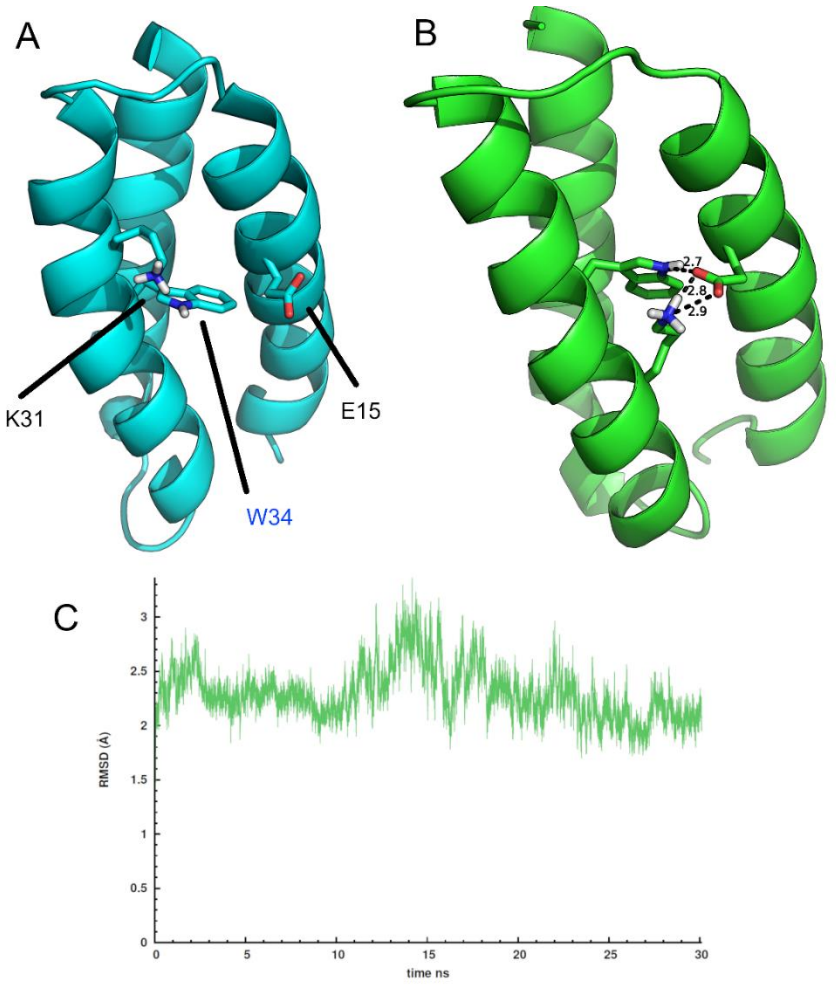

Figure 2.12. NMR structure of α_3W (PDB: 1LQ7) in (A) compared to 30 ns MD model presented in (B). Important residues are labeled in (A); distances are in Ångstroms. (C) The RMSD along the 30 ns simulation of α_3W.

Photochemical generation of W48 produces a stable neutral indole radical (W•), with a half-life of ~7 hours at room temperature.[22] In Nature, the photo-generated tyrosyl radical in photosystem II, Y_D•, lasts for hours[44] and the stable tyrosyl radical in *E. coli* ribonucleotide reductase, Y122•, surrounded by a solvent-excluded pocket, persists for days at room temperature.[45] Conversely, solution tyrosine and tryptophan radicals exist on the microsecond timescale. W108•[28] and α_3W•[17] are moderately-long lived radicals, with decay times of seconds-to-minutes. Previous ^{2}H ENDOR spectroscopic characterization of W108• indicated a weak

hydrogen bond, presumably to water, upon deuterium oxide solvent exchange, while ENDOR analysis of long-lived W48• radical revealed no hydrogen bond interaction.[46] Our MD simulations are consistent with these ENDOR results and provide an atomistic description of the hydrogen-bonding environment surrounding W108 (**Figure 2.10**).

In summary, protein tryptophan sidechains participating in hydrogen bonding, as shown herein (e.g. azurin W108), are associated with conspicuously elevated redox potentials compared to non-hydrogen bonded protein-based tryptophan sidechains. In the context of biological PCET, our study provides an important proof-of-principle glimpse into how changes in non-covalent interactions can tune the local reaction driving forces between amino acid redox pairs and, coupled with proper Marcus reorganization (λ) and distance positioning,[2,3] can control directionality in long-range PCET processes. Resolving these molecular details can expand the developing guidelines for protein engineering.[47]

Methods

Protein Expression and Purification. The genes encoding *Pseudomonas aeruginosa* azurin variants W48 (Y72F/Y108F), W48F (W48F/Y72F/Y108F), and W108 (W48F/Y72F/Y108W) were synthesized by GenScript (Piscataway, NJ) and subcloned into pET 9a vectors. Azurin protein was expressed in and purified from *E. coli* BL21 (DE3) cells as previously described.[48] Briefly, the periplasmic fraction of *E. coli* cell pellet was purified by incubation (37°C, 1.5 h) in resuspension buffer (20 mM potassium phosphate, 2 mM $MgSO_4$, pH 7) supplemented with lysozyme/DNAse I. Cell debris was removed by centrifugation and the solution was adjusted to pH 4.5 using sodium acetate buffer. After removal of aggregate, copper sulfate pentahydrate was added to 20 mM. The protein solution was dialyzed overnight at 4°C in

1 mM sodium acetate, pH 4.5. Azurin was purified to homogeneity, as assessed by a ~14 kDa band in SDS-PAGE (**Figure 2.13**) using a HiTrap SP column attached to AKTA FPLC. Typical yields were ~30 mg/L. UV-vis absorbance spectra of W48 and W108, prepared in our hands (**Figure 2.14**) show characteristic features as previously reported.[23]

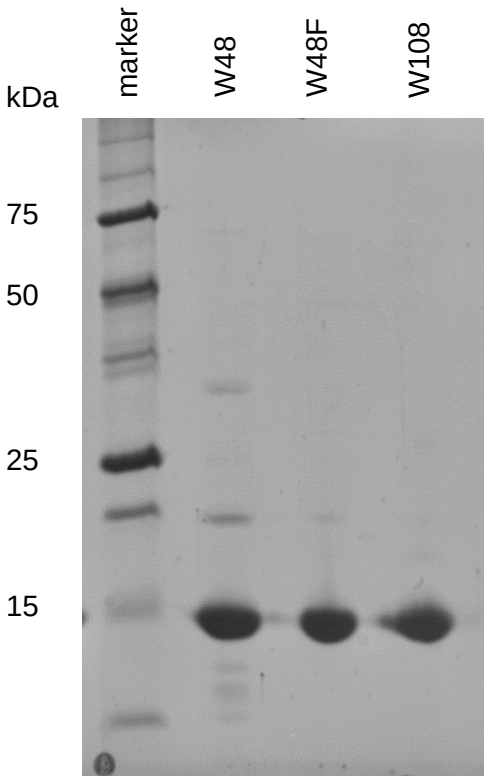

Figure 2.13. SDS PAGE (15%) of azurin variants.

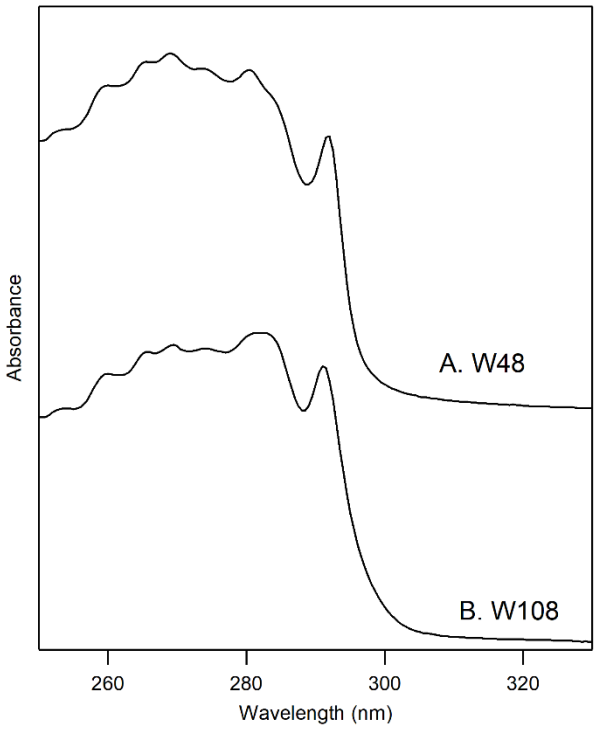

Figure 2.14. Normalized UV-visible absorbance spectra of as-isolated azurin (A) W48 and (B) W108 variants in 25 mM sodium phosphate, pH 7.5 buffer.

As isolated, azurin contains a mixture of Zn^{2+} and Cu^{2+} at the metal binding site. Metal analysis using ICP-OES indicates that the metal molar ratio is 0.6:0.4 Cu^{2+}:Zn^{2+} atoms per azurin monomer. Prior to electrochemistry, the metal was removed by dialysis with cyanide as described previously.[49] The apo form of azurin was incubated with 8 mM zinc sulfate in 20 mM Tris, pH 7.5 buffer twice for one hour each. The pure, Zn^{2+} containing protein ($\geq$ 0.9 Zn^{2+} atoms per monomer by ICP-OES) was concentrated and stored in this Tris buffer at -80°C.

Circular Dichroism. The impact of tryptophan position on the stability of the protein azurin was assessed using CD measurements (Jasco CD spectrometer J-815). The CD spectra of W48, W48F, and W108 were analyzed at room temperature in 10 mM APB

(acetate/phosphate/borate) buffer at pH 7. The concentration was adjusted to 25 μM to ensure the voltage (HT) remained at or lower than 600 V within the spectral range of 190-260 nm. For stability measurements, the wavelength was set to 220 nm and the temperature ranged from 25-90°C. Measurements were taken at an interval of 2°C with a ramp rate of 0.3°C/min and D.I.T. of 8 sec.

Tryptophan and Tyrosine Amino Acid Solution Electrochemistry. N-acetyl-L-tryptophan methyl ester (NAWE) and N-acetyl-L-tyrosine ethyl ester (NAYE) were prepared at 0.2 mM concentrations in 10 mM APB buffer with 200 mM KCl. The solutions were titrated to a range of pH values, from 2 to 13 (by 0.3-0.5 pH increments) using 1 M KOH or 1 M HCl. A CH Instruments (Austin, TX) 600A potentiostat, pyrolytic graphite (PG) working, Pt counter, and saturated calomel (saturated KCl) reference electrodes were used for analysis of these solutions. SWV scans were performed with the following parameters: potential scan range 0 V to 1.1 V, increments of 0.004 V, amplitude of 0.025 V, frequency of 15 Hz, quiet time of 2 sec, and a sensitivity of 1×10^{-5} A.

Immobilization and SWV of Azurin Tryptophan. Pyrolytic graphite electrodes (2 mm-dia.) were polished on a SiC pad, sonicated briefly in water, rinsed with ethanol, and dried under a stream of argon gas. Electrodes were prepared following layer-by-layer (LbL) methods[50-54] to immobilize the protein on the surface: 30 μL drops of poly(diallyldimethylammonium) (PDDA, 2 mg mL^{-1}; 50 mM NaCl), polystyrene sulfonate (PSS, 2 mg mL^{-1}; 50 mM NaCl), and protein were applied for 15 mins each cycle. The following architecture resulted on the electrode surface: $(PDDA/PSS)_2(Protein/PSS)_2$/Protein. The final layer was rinsed with water, and the electrodes were capped and stored at 4°C until use.[8] The presence of the protein on the electrode was analyzed

using a CH Instruments 600A potentiostat with Pt counter and saturated calomel (saturated KCl) reference electrode. SWV scans were performed with the following parameters: potential scan range 0.0 to 1.0 V, step increments of 0.004 V, amplitude of 0.025 V, frequency of 30 Hz, quiet time of 2 sec, and a sensitivity of 1×10^{-5} A. Electrochemical data analysis was performed using Origin Pro software. SWV data were corrected for NHE and background subtracted. The background subtracted data was subjected to 10-point Savitky-Golay smoothing.

Molecular Dynamics. The molecular dynamics were performed with the AMBER 18 suite of programs.[55] For W108, we extracted a monomer from the X-ray structure 1R1C obtained from the Protein Data Bank. A cystine bond was created between the CYS3 and CYS26, all histidine's were defined with a hydrogen on the epsilon nitrogen and the Cu^{1+} was replaced by a Zn^{2+}. The system was solvated with TIP3P waters in a box with a buffer zone of 14 Å. The system was neutralized, and the ionic strength was adjusted to 0.1M by adding sodium and chlorine ions. The non-bonded parameter for Zn^{2+} derived using time-dependent density functional theory[56-57] as outlined in Bartolotti, Pedersen and Charifson.[58] The radius, however, was determined from the calculated electron density as prescribed by Deb, Singh and Sukumar.[59] The system was minimized by combining steepest descent and subsequent conjugate gradient method prior to warming to 300 K. The warming step was performed with NVT dynamics. We found that if we used the SHAKE algorithm in the dynamics, that Zn^{2+} would become unbound to the protein, thus all dynamics were performed without SHAKE and a time step of 1 femtosecond was used. After warming, we performed 50 ps of dynamics in the NPT ensemble to equilibrate the system's density. The Langevin algorithm was employed with a coupling constant of 1.0 ps combined with the Particle mesh Ewald (PME)[60] with a 10 Å cutoff used in the dynamics. The production dynamics was run with the NPT ensemble for nearly 100 ns. The root-mean-square-deviation (RMSD) remained flat

over most of the production dynamics (cf. **Figure 2.10D**). We performed a cluster analysis using CPPTRAJ over the last 30 ns of the simulation. The representative structure taken the from cluster with the smallest distance from the centroid was used in subsequent analysis (**Figure 2.10C**). The starting structure for W48 was obtained by extracting a monomer from the crystal structure 1E67 from the protein data bank. The cystine bridge and histidine's were defined as above for W108. The dynamics involving W48 were performed with Cu^{1+} rather than Zn^{2+}. The reason for this was that, unlike W108, the zinc cation would become unbound from W48 after a few ns of simulation, even with the smaller time step.

References

1. Stubbe, J.: Stubbe, J.; Nocera, D. G.; Yee, C. S.; Chang, M. C., Radical Initiation in the Class I Ribonucleotide Reductases: Long-Range Proton-Coupled Electron Transfer? *Chem. Rev.* **2003**, *103*, 2167-2201.
2. Page, C. C.; Moser, C. C.; Dutton, P. L., Mechanism for Electron Transfer within and between Proteins. *Curr. Opin. Chem. Biol*. **2003**, *7*, 551-556.
3. Gray, H. B.; Winkler, J. R., Long-Range Electron Transfer. *Proc. Natl. Acad. Sci. U.S.A.* **2005**, *102*, 3534-3539.
4. Hammes-Schiffer, S.; Stuchebrukhov, A. A., Theory of Coupled Electron and Proton Transfer Reactions. *Chem. Rev.* **2010,** *110*, 6939-6960.
5. Migliore, A.; Polizzi, N. F.; Therien, M. J.; Beratan, D. N., Biochemistry and Theory of Proton-Coupled Electron Transfer. *Chem. Rev.* **2014,** *114*, 3381-3465.

6. Baldwin, J.; Krebs, C.; Ley, B. A.; Edmondson, D. E.; Huynh, B. H.; Bollinger, J. M., Mechanism of Rapid Electron Transfer During Oxygen Activation in the R2 Subunit of *Escherichia Coli* Ribonucelotide Reductase. 1. Evidence for a Transient Tryptophan Radical *J. Am. Chem. Soc.* **2000,** *122*, 12195-12206.
7. Essenmacher, C.; Kim, S. T.; Atamian, M.; Babcock, G. T.; Sancar, A., Tryptophan Radical Formation in DNA Photolyase: Electron-Spin Polarization Arising from Photoexcitation of a Doublet Ground State. *J. Am. Chem. Soc.* **1993,** *115*, 1602-1603.
8. Aubert, C.; Vos, M. H.; Mathis, P.; Eker, A. P. M.; Brettel, K., Intraprotein Radical Transfer During Photoactivation of DNA Photolyase. *Nature* **2000,** *405*, 586-590.
9. Ruiz-Duenas, F. J.; Pogni, R.; Morales, M.; Giansanti, S.; Mate, M. J.; Romero, A.; Martinez, M. J.; Basosi, R.; Martinez, A. T., Protein Radicals in Fungal Versatile Peroxidase. *J. Biol. Chem.* **2009,** *284*, 7986-7994.
10. Huyett, J. E.; Doan, P. E.; Gurbial, R.; Houseman, A. L.; Sivaraja, M.; Goodin, D. B.; Hoffman, B. M., Coumpound Es of Cytochrome C Peroxidase Contains a Trp Π-Cation Radical: Characterization by Cw and Pulsed Q-Band Endor Spectroscopy. *J. Am. Chem. Soc.* **1995,** *117*, 9033-9041.
11. Wiertz, F. G.; Richter, O.-M. H.; Ludwig, B.; de Vries, S., Kinetic Resolution of a Tryptophan Radical Intermediate in the Reaction Cycle of *Paracoccus Denitrificans* Cytochrome C Oxidase. *J. Biol. Chem.* **2007,** *282*, 31580-31591.
12. Gray, H. B.; Winkler, J. R., Hole Hopping through Tyrosine/Tryptophan Chains Protects Proteins from Oxidative Damage. *Proc. Natl. Acad. Sci. U.S.A.* **2015,** *112*, 10920-10925.

13. Sjodin, M.; Styring, S.; Wolpher, H.; Xu, Y.; Sun, L.; Hammarstrom, L., Switching Redox Mechanism: Models for Proton-Coupled Electron Transfer from Tyrosine and Tryptophan. *J. Am. Chem. Soc.* **2011,** *127*, 3855-3863.
14. Schrauben, J. N.; Cattaneo, M.; Day, T.; Tenderholt, A. L.; Mayer, J. M., Multiple-Site Concerted Proton-Electron Transfer Reactions of Hydrogen-Bonded Phenols Are Nonadiabatic and Well Described by Semiclassical Marcus Theory. *J. Am. Chem. Soc.* **2012,** *134*, 16635-16645.
15. Liu, Z.; Tan, C.; Guo, X.; Li, J.; Wang, L.; Sancar, A.; Zhong, D., Determining Complete Electron Flow in the Cofactor Photoreduction of Oxidized Photolyase. *Proc. Natl. Acad. Sci. U.S.A.* **2013,** *110*, 12966-12971.
16. Berry, B. W.; Martinez-Rivera, M. C.; Tommos, C., Reversible Voltammograms and a Pourbaix Diagram for a Protein Tyrosine Radical. *Proc. Natl. Acad. Sci. U.S.A.* **2012,** *109*, 9739-9743.
17. Glover, S. D.; Tyburski, R.; Liang, L.; Tommos, C.; Hammarström, L., Pourbaix Diagram, Proton-Coupled Electron Trasnfer, and Decay Kinetics of a Protein Tryptophan Radical: Comparing the Redox Properties of W_{32}• and Y_{32}• Generated inside the Structurally Characterized α_3W and α_3Y Proteins. *J. Am. Chem. Soc.* **2018,** *140*, 185-192.
18. Sibert, R.; Josowicz, M.; Porcelli, F.; Veglia, G.; Range, K.; Barry, B. A., Proton-Coupled Electron Transfer in a Biomimetic Peptide as a Model of Enzyme Regulatory Mechanisms. *J. Am. Chem. Soc.* **2007,** *129*, 4393-4400.
19. Shih, C.; Museth, K.; Abrahamsson, M.; Blanco-Rodriguez, A. M.; Di Bilio, A. J.; Sudhamsu, J.; Crane, B. R.; Ronayne, K. L.; Towrie, M.; Vlcek Jr., A.; Richards, J. H.;

Winkler, J. R.; Gray, H. B., Tryptophan-Accelerated Electron Flow through Proteins. *Science* **2008,** *320,* 1760-1762.

20. Warren, J. J.; Herrera, N.; Hill, M. G.; Winkler, J. R.; Gray, H. B., Electron Flow through Nitrotyrosinate in *Pseudomonas Aeruginosa* Azurin. *J. Am. Chem. Soc.* **2013,** *135,* 11151-11158.
21. Takematsu, K.; Williamson, H. R.; Nikolovski, P.; Kaiser, J. T.; Sheng, Y.; Popisil, P.; Towrie, M.; Heyda, J.; Hollas, D.; Zalis, S.; Gray, H. B.; Vlcek Jr., A.; Winkler, J. R., Two Tryptophans Are Better Than One in Accelerating Electron Flow through a Protein. *ACS Cent. Sci.* **2019,** *5,* 192-200.
22. Larson, B. C.; Pomponio, J. R.; Shafaat, H. S.; Kim, R. H.; Leigh, B. S.; Tauber, M. J.; Kim, J. E., Photogeneration and Quenching of Tryptophan Radical in Azurin. *J. Phys. Chem. B* **2015,** *119,* 9438-9449.
23. Shafaat, H. S.; Leigh, B. S.; Tauber, M. J.; Kim, J. E., Spectroscopic Comparison of Photogenerated Tryptophan Radicals in Azurin: Effects of Local Environment and Structure. *J. Am. Chem. Soc.* **2010,** *132,* 9030-9039.
24. Turoverov, K. K.; Kuznetsova, I. M.; Zaitsev, V. N., The Environment of the Tryptophan Residue in *Pseudomonas Aeruginosa* Azurin and Its Fluorescence Properties. *Biophys. Chem.* **1985,** *23,* 79-89.
25. Demchenko, A. P., Red-Edge-Excitation Fluorescence Spectroscopy of Single-Tryptophan Proteins. *Eur. Biophys. J.* **1988,** *16,* 121-129.
26. Finazzi-Agro, A.; Rotilio, G.; Avigliano, L.; Guerrieri, P.; Boffi, V.; Mondovi, B., Environment of Copper in *Pseudomonas Fluorescens* Azurin: Fluorometric Approach. *Biochemistry* **1970,** *9,* 2009-2014.

27. Broos, J.; Tveen-Jensen, K.; de Waal, E.; Hesp, B. H.; Jackson, J. B.; Canters, G. W.; Callis, P. R., The Emiting State of Tryptophan in Proteinswith Highly Blue-Shifted Fluorescence. *Angew. Chem. Int Ed.* **2007,** *46*, 5137-5139.

28. Miller, J. E.; Gradinaru, C.; Crane, B. R.; Di Bilio, A. J.; Wehbi, W. A.; Un, S.; Winkler, J. R.; Gray, H. B., Spectroscopy and Reactivity of Photogenerated Tryptophan Radical in a Structurally Defined Protein Environment. *J. Am. Chem. Soc.* **2003,** *125*, 14220-14221.

29. Di Bilio, A. J.; Chang, T. K.; Malmstrom, B. G.; Gray, H. B.; Karlsson, G.; Nordling, M.; Pascher, T.; Lundberg, L. G., Electronic Absorption Spectra of M(Ii)(Met121x) Azurins (M=Co, Ni, Cu; X = Leu, Gly, Asp, Glu): Charge-Transfer Energies and Reduction Potentials. *Inorg. Chim. Acta* **1992,** *198-200*, 145-148.

30. Marshall, N. M.; Garner, D. K.; Wilson, T. D.; Gao, Y.-G.; Robinson, H.; Nilges, M. J.; Lu, Y., Rationally Tuning the Reduction Potential of a Single Cupredoxin Beyond the Natural Range. *Nature* **2009,** *462*, 113-116.

31. Monari, S.; Battistuzzi, G.; Bortolotti, C. A.; Yanagisawa, S.; Sato, K.; Li, C.; Salard, I.; Kostrz, D.; Borsari, M.; Ranieri, A.; Dennison, C.; Sola, M., Understanding the Mechanism of Short-Range Electron Transfer Using an Immobilized Cupredoxin. *J. Am. Chem. Soc.* **2012,** *134*, 11848-11851.

32. Jeuken, L. J. C.; Armstrong, F. A., Electrochemical Origins of Hysteresis in the Electron-Transfer Reactions of Adsorbed Proteins: Contrasting Behavior of the "Blue" Copper Protein, Azurin, Adsorbed on Pyrolytic Graphite and Modified Gold Electrodes. *J. Phys. Chem. B* **2001,** *105*, 5271-5282.

33. Lancaster, K. M.; DeBeer, S.; Yokoyama, K.; Richards, J. H.; Gray, H. B., Type-Zero Copper Proteins. *Nat. Chem.* **2009,** *1*, 711-715.

34. Tommos, C.; Valentine, K. G.; Martinez-Rivera, M. C.; Liang, L.; Moorman, V. R., Reversible Phenol Oxidation and Reduction in the Structurally, Well-Defined 2-Mercaptophenol-A_3c Protein. *Biochemistry* **2013,** *52*, 1409-1418.

35. Ravichandran, K. R.; Zong, A. B.; Taguchi, A. T.; Nocera, D. G.; Stubbe, J.; Tommos, C., Formal Reduction Potentials of Difluorotyrosine and Trifluorotyrosine Protein Residues: Defining the Thermodynamics of Multistep Radical Transfer. *J. Am. Chem. Soc.* **2017,** *139*, 2994-3004.

36. Harriman, A., Further Comments on the Redox Potentials of Tryptophan and Tyrosine. *J. Phys. Chem.* **1987,** *91*, 6102-6104.

37. Mahmoudi, L.; Kissner, R.; Nauser, T.; Koppenol, W. H., Electrode Potentials of L-Tryptophan, L-Tyrosine, 3-Nitro-L-Tyrosine, 2,3-Difluoro-L-Tyrosine, and 2,3,5-Trifluoro-L-Tyrosine. *Biochemistry* **2016,** *55*, 2849-2856.

38. Tommos, C.; Skalicky, J. J.; Pilloud, D. L.; Wand, A. J.; Dutton, P. L., De Novo Proteins as Models of Radical Enzymes. *Biochemistry* **1999,** *38*, 9495-9507.

39. Surewicz, W. K.; Szabo, A. G.; Mantsch, H. H., Conformational Properties of Azurin in Solution as Determined from Resolution-Enhanced Fourier-Transform Infrared Spectra. *Eur. J. Biochem.* **1987,** *167*, 519-523.

40. Nar, H.; Huber, R.; Messerschmidt, A.; Filippou, A. C.; Barth, M.; Jaquinod, M.; Van De Kamp, M., Characterization and Crystal Structure of Zinc Azurin, a by-Product of Heterologous Expression in *Escherichia Coli* of *Pseudomonas Aeruginosa* Copper Azurin. *Eur. J. Biochem.* **1992,** *205*, 1123-1129.

41. Miura, T.; Takeuchi, H.; Harada, I., Characterization of Individual Tryptophan Side Chains in Proteins Using Raman Spectroscopy and Hydrogen-Deuterium Exchange Kinetics. *Biochemistry* **1988,** *27*, 88-94.

42. Dai, Q.-H.; Tommos, C.; Fuentes, E. J.; Blomberg, M. R.; Dutton, P. L.; Wand, A. J., Structure of a *De Novo* Designed Protein Model of Radical Enzymes. *J. Am. Chem. Soc.* **2002,** *124*, 10952-10953.

43. Miller, M. A.; Han, G. W.; Kraut, J., A Cation Binding Motif Stabilizes the Compound I Radcial of Cytochrome C Peroxidase. *Proc. Natl. Acad. Sci. U.S.A.* **1994,** *91*, 11118-11122.

44. Barry, B. A., Proton Coupled Electron Transfer and Redox Active Tyrosines in Photosystem Ii. *J. Photochem. Photobiol. B* **2011,** *104*, 60-71.

45. Ormo, M.; Regnstrom, K.; Wang, Z.; Que Jr., L.; Sahlin, M.; Sjoberg, B.-M., Residues Important for Radical Stability in Ribonucleotide Reductase from *Escherichia Coli*. *J. Biol. Chem.* **1995,** *270*, 6570-6576.

46. Stoll, S.; Shafaat, H. S.; Krzystek, J.; Ozarowski, A.; Tauber, M. J.; Kim, J. E.; Britt, R. D., Hydrogen Bonding of Tryptophan Radicals Revealed by Epr at 700 Ghz. *J. Am. Chem. Soc.* **2011,** *133*, 18098-18101.

47. Smith, A. T.; Doyle, W. A.; Dorlet, P.; Ivancich, A., Spectroscopic Evidence for an Engineered, Catalytically Active Trp Radical That Creates Unique Reactivity of Lignin Peroxidase. *Proc. Natl. Acad. Sci. U.S.A.* **2009,** *106*, 16084-16089.

48. Piccioli, M.; Luchinat, C.; Mizoguchi, T. J.; Ramirez, B. E.; Gray, H. B.; Richards, J. H., Paramagnetic Nmr Spectroscopy and Coordination Structure of Cobalt(Ii) Cys112asp Azurin. *Inorg. Chem.* **1995,** *34*, 737-742.

49. Mei, G.; Di Venere, A.; Campeggi, F. M.; Gilardi, G.; Rosato, N.; De Matteis, F.; Finazzi-Agro, A., The Effect of Pressure and Guanidine Hydrochloride on Azurins Mutated in the Hydrophobic Core. *Eur. J. Biochem.* **1999,** *265*, 619-626.

50. Lvov, Y. M.; Lu, Z.; Schenkman, J. B.; Zu, X.; Rusling, J. F., Direct Electrochemistry of Myoglobin and Cytochrome $P450_{cam}$ in Alternate Layer-by-Layer Films with DNA and Other Polyions. *J. Am. Chem. Soc.* **1998,** *120*, 4073-4080.

51. Rusling, J. F., Electroactive and Enzyme-Active Protein-Polyion Films Assembled Layer-by-Layer. In *Protein Architecture: Interfacing Molecular Assemblies and Immobilization Biotechnology*, Lvov, Y.; Mohwald, H., Eds. Marcel Dekker: New York, 2000; pp 337-354.

52. Lvov, Y.; Ariga, K.; Ichinose, I.; Kunitake, T., Assembly of Multicomponent Protein Films by Means of Electrostatic Layer-by-Layer Adsorption. *J. Am. Chem. Soc.* **1995,** *117*, 6117-6123.

53. Rusling, J. F.; Hvastkovs, E. G.; Hull, D. O.; Schenkman, J. B., Biochemical Applications of Ultrathin Films of Enzymes, Polyions and DNA. *Chem. Commun.* **2008**, 141-154.

54. Panchagnula, V.; Kumar, C. V.; Rusling, J. F., Ultrathin Layered Myoglobin-Polyion Films Functional and Stable at Acidic Ph Values. *J. Am. Chem. Soc.* **2002,** *124*, 12515-12525.

55. Case, D. A.; Ben-Shalom, I. Y.; Brozell, S. R.; Cerutti, D. S.; Cheatum III, T. E.; Cruzeiro, V. W. D.; Darden, T. A.; Duke, R. E.; Ghoreishi, D.; Gilson, M. K.; Gohlke, H.; Goetz, A. W.; Greene, D.; Harris, R.; Homeyer, N.; Izadi, S.; Kovalenko, A.; Kurzman, T. K.; Lee, T. S.; LeGrand, S.; Li, P.; Lin, C.; Liu, J.; Luchko, T.; Luo, R.;

Mermelstein, D. J.; Merz, K. M.; Miao, Y.; Monard, G.; Nguyen, C.; Nguyen, H.; Omelyan, I.; Onufriev, A.; Pan, F.; Qi, R.; Roe, D. R.; Roitberg, A.; Sagui, C.; Schott-Verdugo, S.; Shen, J.; Simmerling, C. L.; Smith, J.; Salomon-Ferrer, R.; Swails, J.; Walker, R. C.; Wang, J.; Wei, H.; Wolf, R. M.; Wu, X.; Xiao, L.; York, D. M.; Kollman, P. A. *Amber*, University of California, San Francisco, 2018.

56. Bartolotti, L. J., Time-Dependent Extension of the Hohenberg-Kohn-Levy Energy-Density Functional. *Phys. Rev. A* **1981,** *24*, 1661-1667.
57. Bartolotti, L. J., Time-Dependent Kohn-Sham Density-Functional Theory. *Phys. Rev. A* **1982,** *26*, 2243-2244.
58. Bartolotti, L. J.; Pedersen, L. G.; Charifson, P. S., Long Range Nonbonded Attractive Constants for Some Charged Atoms. *J. Comp. Chem.* **1991,** *12*, 1125-1128.
59. Deb, B. M.; Singh, R.; Sukumar, N., A Universal Density Criterion for Correlating the Radii and Other Properties of Atoms and Ions. *J. Mol. Structure* **1992,** *259*, 121-139.
60. Darden, T.; York, D.; Pedersen, L., Particle Mesh Ewald: A *N* Log(*N*) Method for Ewald Sums in Large Systems. *J. Chem. Phys.* **1993,** *98*, 10089.

CHAPTER 3

Influence of Local Electrostatics on the Reduction Potentials of Tryptophan and Tyrosine in Engineered Azurin Variants

Introduction

Tyrosine and tryptophan amino acids play critical roles in mediating high-potential redox reactions by facilitating long-range electron transfer.[1] Tyrosine mediated PCET is very common and tyrosyl radicals, formed by oxidation, have been observed in cytochrome c oxidase photosystem II, ribonucleotide reductase (RNR), cyclooxygenase, and fatty acid α-oxygenase.[2] Tryptophan is a less abundant amino acid, but is seen to be found in higher abundance in oxidoreductases. In select systems, such as DNA photolyase, cytochromes, and engineered peroxidase, a string of tryptophan residues play a critical role in mediating PCET. Both tyrosine and tryptophan residues have been implicated in redox 'wires' that may prevent oxidative damage.[3]

In select systems, including RNR, reversible electron transfer is needed to maintain the integrity of the enzyme.[4] While the predominant barrier for electron transfer arises from the environmental reorganization energy (λ) from Marcus theory, the reversibility of electron transfer is anticipated to be controlled by the local driving forces.[5] This means that the local environment is expected to modulate the reduction potentials of the specific amino acid radicals to control directionality of electron flow. In complex systems, direct detection of a specific amino acid radical is considerably challenging due to the potential overlap and contributions from other undesired amino acids. To overcome these limitations, model systems have been exploited. As presented in Chapter 1 of this thesis, there have been two research groups (Barry and Tommos) with opposing

strategies that have set to address the impact of the protein environment on the reduction potentials of tryptophan and tyrosine.

Chapter 2 presented a proof-of-principle demonstration that the single tryptophan-containing protein, azurin, can be examined using square wave electrochemistry (**Figure 3.1A**). Using two previously characterized variants, W48 and W108, which exhibit different spectroscopic properties consistent with a rigid, solvent-excluded and more solvent-accessible environments, respectively, it was shown that the reduction potential of the tryptophan radical is sensitive to local electrostatics (**Figure 3.1B**).[6] In this chapter, the study is expanded to new engineered azurin variants in which the tryptophan is in variable degrees of hydrogen bonding and solvent exposure. Further, we extend the analysis to tyrosine. The tryptophan residue at W48 is substituted for tyrosine and compared to a previously engineered variant, Y48/H20 in which a histidine is introduced into the hydrophobic cavity of azurin and was shown to form a strong hydrogen bond with Y48 phenol group.[7] This chapter presents electrochemical, spectroscopic and crystallographic data for these new variants. The data provides new information into how the local polarity and hydrogen bonding microenvironments influence the reduction potentials of tyrosine and tryptophan in proteins.

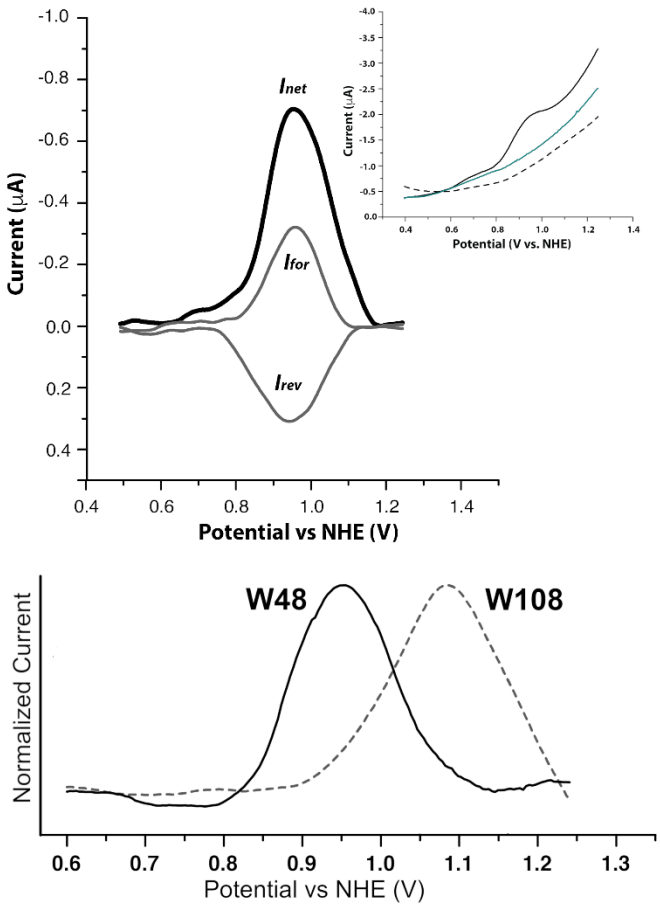

Figure 3.1. SWV response of azurin W48 and the forward and reverse current of the net electrochemical response at pH 7 (A). Raw SWV are presented in the inset. (B) SWV-detected difference in the reduction potentials between azurin W48 and W108 proteins in which the tryptophan is in a nonpolar and polar environment, respectively.

Methods

Azurin Mutant Expression and Purification. The genes encoding *Pseudomonas aeruginosa* azurin variants W48/F110S (W48/Y72F/Y108F/F110S), W48/F110L (W48/Y72F/Y108F/F110L), W48/F110A (W48/Y72F/Y108F/F110A), Y48 (W48Y/Y72F/Y108F), Y48/H20 (W48Y/Y72F/Y108/H20), and Y108 (W48F/Y72F/Y108) were synthesized by GenScript (Piscataway, NJ) and subcloned into pET 9a vectors. Azurin protein was expressed in and purified from *E. coli* BL21 (DE3) cells as previously described.[6] Azurin was

purified to homogeneity from a semi-purified periplasmic fraction using a HiTrap SP column attached to AKTA FPLC. Typical yields were 10-30 mg/L. Protein purity was characterized by SDS-PAGE. Using this method, the protein contains a mixture of Cu^{2+} and Zn^{2+}. Because our previous SWV results indicated no significant difference in the reduction potentials of W48 in Cu^{2+} or Zn^{2+} containing forms of azurin, no further steps were taken to reconstitute the protein.

CD Spectroscopy to Determine Protein Stability. The impact of tryptophan position on the stability of the protein azurin was assessed using CD measurements (Jasco CD spectrometer J-815). The CD spectra of azurin mutants were analyzed at room temperature in 10 mM APB (acetate/phosphate/borate) buffer at pH 7 and pH 9. The concentration was adjusted to 25 μM to ensure the voltage (HT) remained at or lower than 600 V within the spectral range of 190-260 nm. For stability measurements, the wavelength was set to 220 nm and the temperature ranged from 25-90°C. Measurements were taken at an interval of 2°C with a ramp rate of 0.3°C/min and D.I.T. of 8 sec.

Immobilization and SWV of Azurin Tryptophan and Tyrosine Mutants. Pyrolytic graphite electrodes (2 mm-dia.) were polished on a SiC pad, sonicated briefly in water, rinsed with ethanol, and dried under a stream of argon gas. Electrodes were prepared following layer-by-layer (LbL) methods to immobilize the protein on the surface: 30 μL drops of poly(diallyldimethylammonium) (PDDA, 2 mg mL^{-1}; 50 mM NaCl), polystyrene sulfonate (PSS, 2 mg mL^{-1}; 50 mM NaCl), and protein were applied for 15 mins each cycle. The following architecture resulted on the electrode surface: PDDA/PSS/$(Protein/PSS)_2$/Protein. The final layer was rinsed with water, and the electrodes were capped and stored at 4°C until use. The presence of the protein on the electrode was analyzed using a CH Instruments 600A potentiostat with Pt

counter and saturated calomel (saturated KCl) reference electrode. SWV scans were performed with the following parameters: potential scan range 0.0 to 1.0 V (vs SCE), step increments of 0.004 V, amplitude of 0.025 V, frequency of 200 Hz, quiet time of 2 sec, and a sensitivity of 1×10^{-5} A. Origin Pro software was used to analyze electrochemical data, and the data was background subtracted, subjected to 15-point Savitky-Golay smoothing, and corrected for NHE.

X-ray Crystallography. Protein aliquots were thawed on ice. Various samples were prepared to determine the best solution condition for crystal formation. Current results suggest that 0.2 M sodium formate (2M), 0.1M HEPES buffer (1M), and various concentrations of PEG 3350 (50%) are best, with certain proteins requiring 0.2M ammonium chloride (2M) rather than sodium formate. Plates were left to sit for 1 week before checking for crystals. The diffraction pattern was collected at the Argonne National Labs using the Synchrotron.

Results and Discussion

Select azurin mutants were designed with the intent to increase the polarity surrounding W48, a tryptophan in the native azurin protein that is structurally rigid and in a non-polar environment (**Figure 3.2A-B**). There was already information regarding the results of F110S and F110A mutations on the protein structure. X-ray structure of F110S suggested the presence of water molecules in the cavity surrounding W48.[8] Whereas, the steady-state fluorescence of F110A indicated W48 would experience the impact of a polar environment without the possibility of hydrogen bonds within the inner cavity.[9] These variants acted as a baseline for the reduction potential studies in this chapter. To further understand the impact of cavity size and polarity on the W48 potentials, azurin was also mutated to W48/F110L (**Figure 3.2B**). Leucine is much larger than alanine and serine and should maintain a non-polar environment.

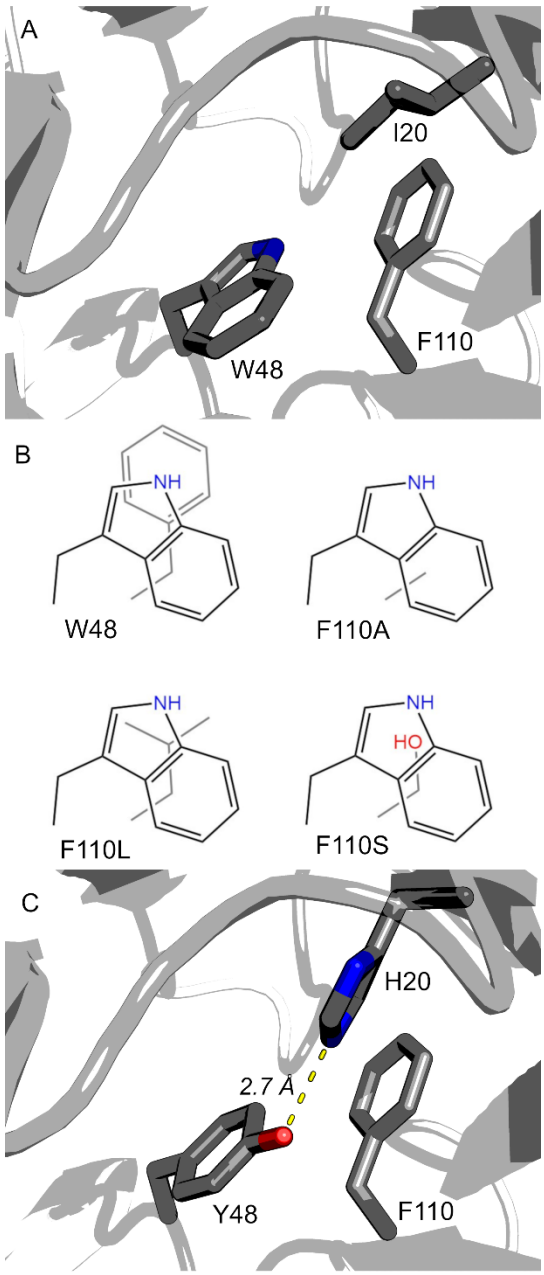

Figure 3.2. Designed Azurins. X-ray structure of wild-type azurin (PDB: 1E67) in (A). In (B), modified azurins to investigate the effect of the local environment around W48, studied herein. Panel (C) shows the X-ray structure of the engineered Y48/H20 (W48Y/I20H) azurin variant, in which histidine at position 20 forms a strong hydrogen bond with Y48.

These studies were extended to also include engineered Y48 azurin variants. Recently, Harry Gray's group reported an engineered Y48/I20H (Y48/H20) variant that substituted W48 for tyrosine and incorporated a strong hydrogen bond upon the introduction of a histidine at position 20 (**Figure 3.2C**).[7]

These proteins (**Figure 3.2**) were expressed and purified from *E. coli* cultures as described in Chapter 2. The UV-visible and fluorescence spectra of the purified tryptophan variants were collected at pH 7 and presented in **Figure 3.3A-D**. In all cases, the UV signature exhibits fine structure consistent with a rigid protein in a well folded, nonpolar environment. This is validated by the comparison to indole in solvents with varying polarity (**Figure 3.3E-H**). Indole dissolved in low dielectric solvent (e.g. cyclohexane) shows fine structure in the UV-vis spectrum. The peak emission wavelength of tryptophan is known to be a strong marker for the polarity of its environment. This is seen by the significant shift in the indole peak emission from 350 nm in water ($\varepsilon = 80$) to 332 nm in ethanol ($\varepsilon = 25$) and to 300 nm in cyclohexane ($\varepsilon = 2$). The addition of hexamethylphosphoramide (HMPA), a proton acceptor, in cyclohexane shifted this peak to 310 nm, providing proof-of-principle into the ability for fluorescence to quantify polarity in non-homogenous environments. In azurin, the peak emission wavelenghts were different. W48, the wildtype protein, has an emission of 308 nm, which is the most blue shifted wavelength in a natural protein. This result is consistent with its previously characterized X-ray structure (**Figure 3.2A**), in which the tryptophan is buried in a rigid and solvent-free beta barrel. Conversely, W108 exhibits red-shifted emission peak at 340 nm. While there is no X-ray structure of W108, our group previously carried out 30 ns MD simulations on the *in silico* structure (see Chapter 2). From this model, the indole nitrogen of W108 is solvent accessible and forms a hydrogen bond interaction with a water network that leads to the surface of the protein. This MD model supports the apparent

increase in polarity in W108 as implicated from the λ_{em}. In addition to these two previously characterized azurin protein variants, we constructed W48 mutants with F110S, F110A, and F110L. The λ_{em} values for the former two variants are identical at 322 nm, a value that lies in between the λ_{em} values for W48 (308 nm) and W108 (340 nm). Note that the fluorescence emission spectrum of W48/F110L was completely quenched, despite a scan of the excitation wavelength (λ_{ex}) and buffer solutions. These fluorescence data suggest that altering the bulk at the cross-strand Phe to volume reducing sidechains results in red-shifted fluorescence maxima supporting enhanced polarity in the cavity.

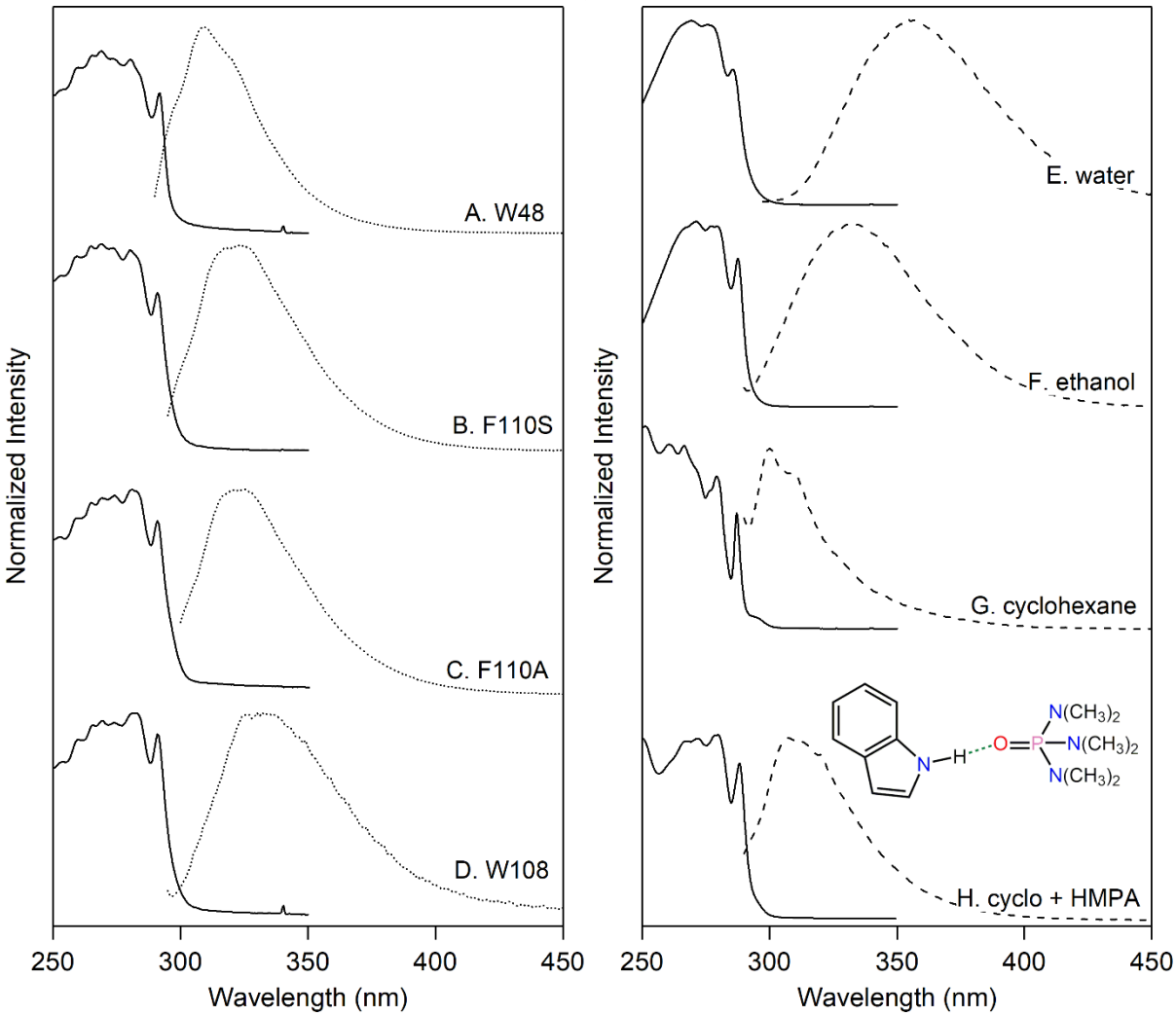

Figure 3.3. UV/Vis, fluorescence of W48 F110X (A-D) and indole model spectra (E-H). The protein solutions were prepared at 20 μM in 25 mM phosphate, pH 7 for UV/vis. For fluorescence, the protein samples were diluted to 5 μM. The excitation wavelength for the azurin fluorescence spectra was 290 nm. For the model spectra (E-H), the solutions were prepared at 200 uM in their respective solvents. In (H), 0.08% (v/v) of the proton acceptor, HMPA was added to cyclohexane.

Table 3.1. Fluorescence Emission Maxima for Azurin Tryptophan Variants (from **Figure 3.3**)

	λ_{em} (nm)
W48	309
W48/F110S	322
W48/F110L	N.D.
W48/F110A	322
W108	335
α_3W	325
W (soln)	355

To rule out artificactual shifts in λ_{em} from protein instability/unfolding, circular dichroism (CD) spectroscopy was performed to confirm secondary structure (**Figure 3.4**). Azurin variants exhibited the typical CD trace of a predominantly β sheet secondary structure of azurin, though the W48 variants with polar environments (e.g. F110S) exhibited slight shifts in the CD spectrum. The latter could be attributed to a slight structural shift in the tertiary structure. The melting temperature (T_m) of the protein can be determined by locking the CD wavelength at 220 nm and scanning as a function of temperature. The CD-derived T_m values, listed in **Table 3.2**, report on the thermal stability of the protein structure. To corroborate these results and provide more thermodynamic information for the thermal stability of azurin variants, differential scanning calorimetry (DSC) was performed. Representative DSC curves are presented in **Figure 3.5**. The T_m values were determined by the peak in the DSC traces and the area of the curves report on the enthalpy; these values are listed in **Table 3.2**. Note that the T_m values from DSC are systematically higher than the values determined by CD. The DSC derived T_m and ΔH values for the W48 variant are consistent with previous literature values.[10] While the W48 variants F110A and F110S had lower Tm values compared to W48, their enthalpy values were within range for that reported for other azurin mutants that maintain copper-mediated ET reactivity.[11] Note that an extreme case is

W48/F110L which despite a moderate T_m value of 57-59 °C, the enthalpy is greatly reduced to 58 ± 2 from 470 ± 15 kJ/mol in W48. These data support that the F110L mutant is not very stable and will not be studied further for its electrochemical/spectroscopic properties.

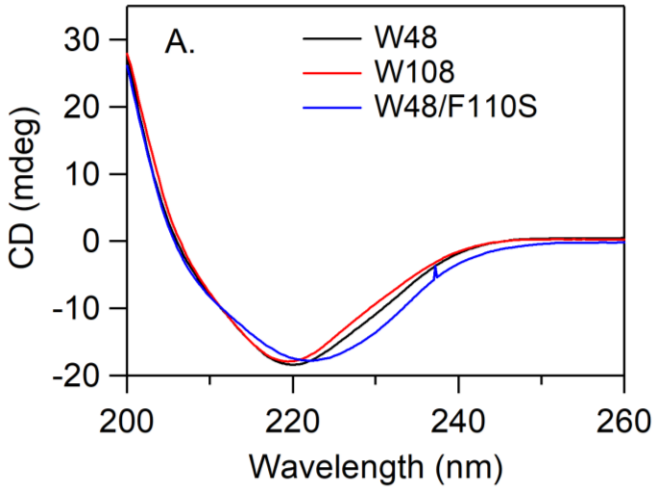

Figure 3.4. CD traces of W48, W108, and W48/F110S variants at 25 °C. Samples were prepared at 25 mM concentrations in 25 mM phosphate pH 7 buffer.

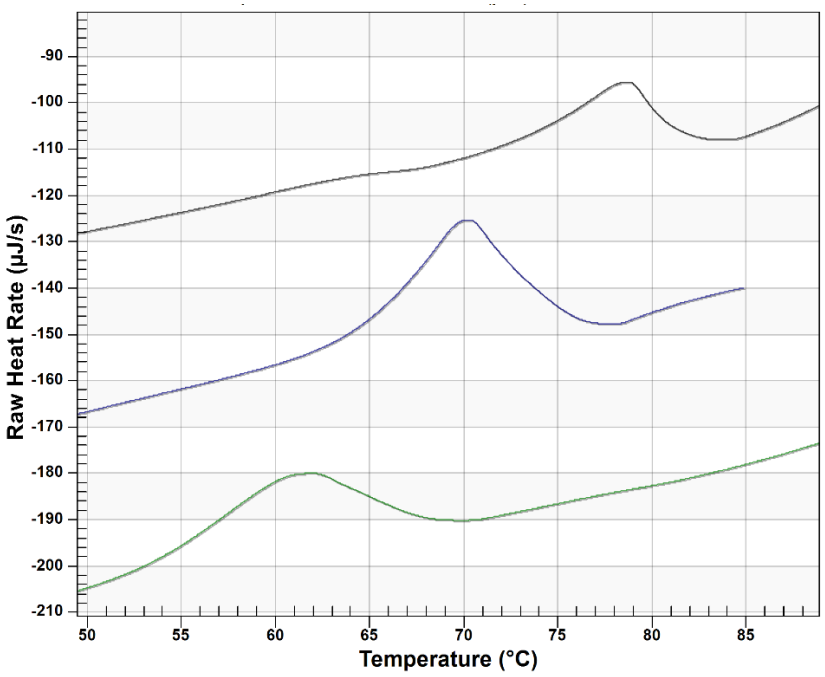

Figure 3.5. Representative DSC traces of W48 (black), W108 (blue) and W48/F110S (green) variants. The protein concentrations were 0.6-1.4 mg/mL in 25 mM phosphate, pH 7 buffer.

Table 3.2. Thermodynamic and Electrochemical Parameters of Azurin Variants

	Tm (°C) CD	Tm (°C) DSC	ΔH (kJ/mol)	*E* (mV)	
				pH 7	pH9
W48	74.0 ± 0.7	78.1 ± 0.5	470 ± 15	952 ± 6	849 ± 8
W48/F110S	54.3 ± 0.3	61.3 ± 0.3	337 ± 15	1028 ± 14	890 ± 2
W48/F110L	57.3 ± 0.2	59.4 ± 0.2	58 ± 2	N.D.	904 ± 4
W48/F110A	58.4 ± 0.2	61.2 ± 0.1	334 ± 26	N.D.	896 ± 10
W108	67.4 ± 0.2	70.1 ± 0.3	392 ± 31	1070 ± 8	938 ± 12
α_3W	49	49	43	1134 ± 16 (1095 ± 4)	N.M.
Y48	69.6 ± 0.1; pH 7 65.9 ± 0.1; pH 9	69.6 ± 0.1; pH 7 65.9 ± 0.1; pH 9	289 ± 4 155 ± 4	976 ± 10	882 ± 8
Y48/H20	47.9 + 0.5; pH 9	55.3 ± 0.1; pH 9		N.M.	920 ± 15

N.D. = not detected. N.M. = Not measured. Buffer was 25 mM phosphate, pH 7 and 25 mM borate, pH 9.

SWV was collected for W48/F110S and F110A at pH 7 and 9. These values are listed in **Table 3.2** and compared to the values previously collected for W48 and W108 (Chapter 2). The peak potentials from the background-subtracted square wave voltammograms for these azurin variants are plotted against their λ_{em} wavelength and presented in **Figure 3.6**. At pH 7, the electrochemical potentials for W48, W48/F110S, and W108 are well correlated with the polarity of the tryptophan sidechain as assessed by their fluorescence emission wavelength. The previously characterized tryptophan in a *four-helix* bundle, α4W,[12] also tracks well with this correlation, despite very different protein scaffold structures. In contrast, the tryptophan in a *three-helix* bundle, α3W,[13] has an anomalously high reduction potential for a protein-derived tryptophan and does not fit with the correlation. At pH 9, the electrochemical potentials of W48, F110S, F110A, and W108 are well correlated. Note that F110L was excluded from this analysis as the fluorescence spectrum was quenched and thus the peak emission could not be determined.

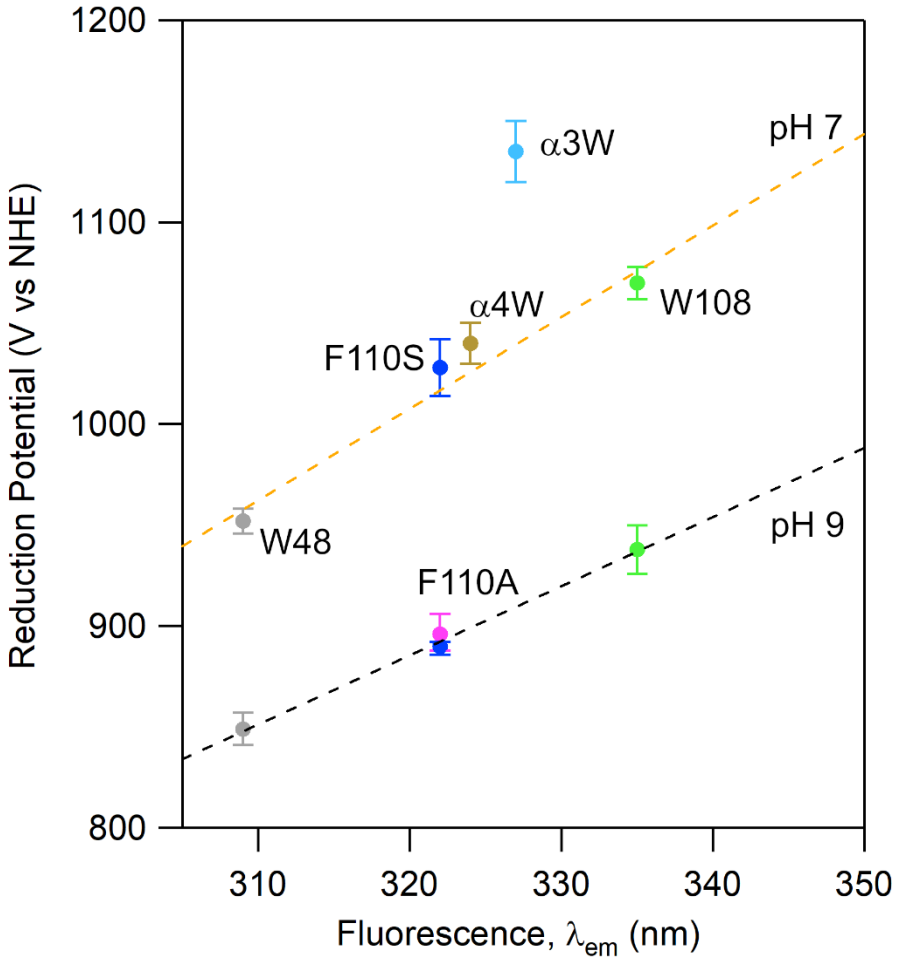

Figure 3.6. SWV peak potentials of these azurin variants at pH 7 (orange dashed line) and pH 9 (black dashed line) plotted versus the fluorescence maximum. The azurin variants are color-coded. In addition, the reduction potentials of the artificial helical bundle proteins, α3W[13] and α4W[12], characterized by the Tommos group were plotted.

To provide a physical basis for the observed differences in the fluorescence spectra and to rationalize the SWV results, **Figure 3.7** presents the cryogenic X-ray structures of the various W48 azurin variants. W48 and W48/F110S had been previously determined (**Figure 3.7A** and **B**, respectively).[8,14] Compared to W48, the substitution of the cross-strand phenylalanine leads to the introduction of water molecules into the cavity generated by reducing the bulk of Phe to the polar sidechain of serine. In collaboration with Prof. Choe at ECU, we prepared azurin crystals and

obtained high-resolution structural models of the F110L (**Figure 3.7C**) and F110A (**Figure 3.7D**) variants of azurin.

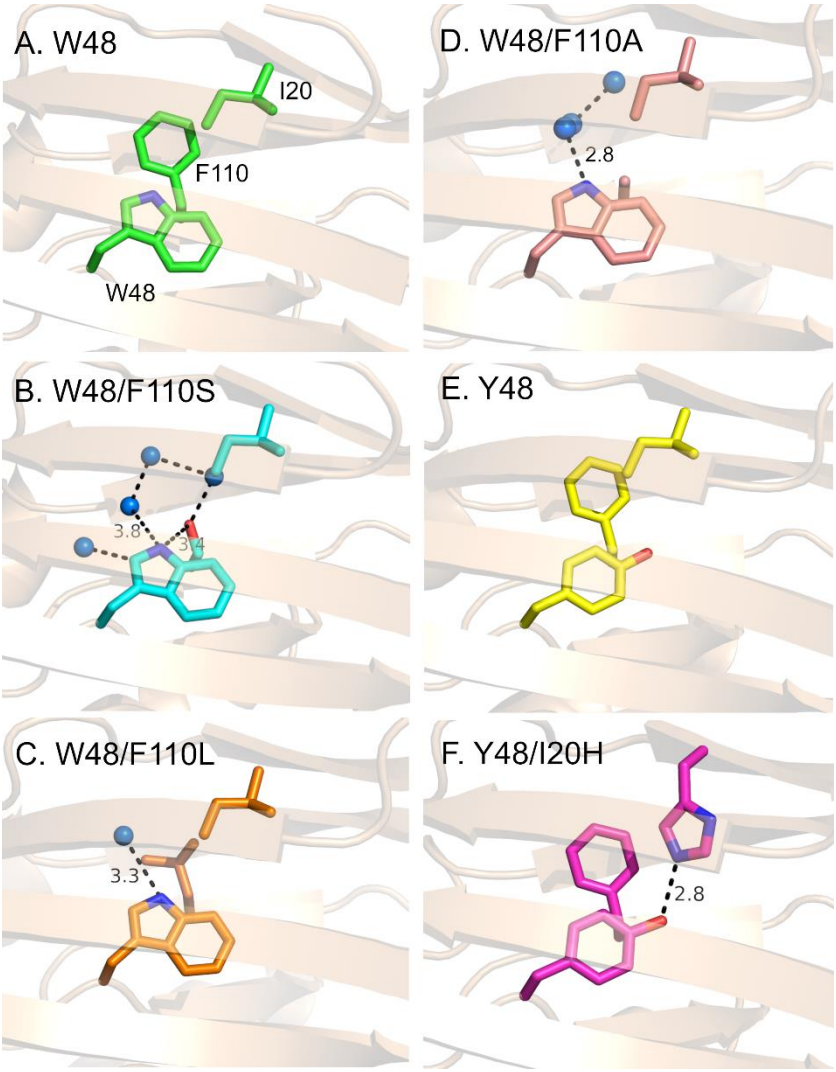

Figure 3.7. X-ray structural models of the environment surrounding W48 or Y48. The structures represent 2.14 (PDB: 1E67), 2.3 (PDB: 1ILU), 1.25, 1.15, 1.3, and 1.18 (PDB: 3U25) Å resolution, respectively. Crystallographically resolved water molecules inside the azurin cavity are represented by blue spheres. Distances are in Å. See **Table 3.3** for crystal data statistics.

Table 3.3. Statistics of Crystal Data Collection and Refinement for Azurin Mutants

Data	110A	110L	Y48
PDB ID			
Resolution range (Å)	50 – 1.25	50 – 1.15	50 – 1.30
Space group	P 2_1	P 2_1 2_1 2_1	P 2_1 2_1 2
Unit cell (Å)	49.43, 64.82, 71.15	48.17, 66.73, 69.81	49.82, 60.37, 71.90
Unit cell (deg)	90, 90.92, 90	90, 90, 90	90, 90, 90
Wavelength (Å)	1.0	0.97934	1.03315
Beam lines	SBC-CAT, APS	SBC-CAT, APS	GM/CA-CAT, APS
Number of measurements	363750	494030	199980
Number of unique reflections	117338	78418	48778
Completeness of data (%)			89.3
Overall	95.7	97.3	40.4 (1.32 –
Shell/resolution range (Å)	93.1 (1.27 – 1.25)	76.8 (1.17 - 1.15)	1.30)
R_{sym} (%)			6.2
Overall	5.9	8.6	44.2 (1.32 –
Last shell/resolution range (Å)	59.8 (1.27 – 1.25)	35.7 (1.17 - 1.15)	1.30)
CC1/2	0.690 (1.27 –		0.525 (1.32 –
Last shell/resolution range (Å)	1.25)	0.908 (1.17 - 1.15)	1.30)
I/sigma			36.3
Overall	22.9	35.9	1.70 (1.32 –
Last shell/resolution range (Å)	1.60 (1.27 – 1.25)	3.62 (1.17 - 1.15)	1.30)
Wilson B-factor	11.83	7.71	10.59
R_{work}	13.43	14.07	15.41
R_{free}	16.07	15.63	17.74
Number of atoms	3706	2405	2240
Macromolecules	3850	1936	1938
Ligands	4	12	2
Solvent	852	457	300
Mean B (Å^2)	17.85	12.95	18.56
RMS (bonds)	0.010	0.008	0.008
RMS (angles)	1.09	1.03	0.92
Ramachandran favored (%)	99.0	98.81	99.21
Ramachandran allowed (%)	1.0	1.19	0.79
Ramachandran outliers (%)	0	0	0
Rotamer outliers (%)	0	0	0

$R_{sym} = \Sigma_j \Sigma_i |I_{ij} - \langle I_j \rangle| / \Sigma_i \Sigma_j I_{ij}$, where i runs over multiple obervations of the same intensity, and j runs over all crystallographic unique intensities. $R_{factor} = \Sigma ||F_{obs}| - |F_{calc}|| / \Sigma |F_{obs}|$. R_{free} was calculated with 5% of the reflections selected.

Note that the newly solved structures of F110L and F110A (**Figure 3.7C-D**) also show infiltration of water molecules (blue spheres) into the azurin beta barrel cavity. The structural effect from reducing the sidechain bulk at Phe110 to smaller aliphatic residues (Ala or Leu) is like that observed by F110S. This includes the Phe→Leu mutation. The impaired structural stability of the F110L as seen in the significantly reduced T_m and ΔH from DSC experiments could be attributed to the penetration of high-energy or 'frustrated' water molecules.[15,16]

Tyrosine in azurin. The UV/Vis of the purified Y protein variants were collected at pH 7 (**Figure 3.8**). The sharp absorption peaks around ~280 nm observed for the newly engineered Y48 (**Figure 3.8A**) disappear in the Y48/H20 and Y108 spectra (**Figure 3.8B-C**). Based on comparisons to solution spectra of p-cresol - the structural mimic of the tyrosine sidechain in various solvents (**Figure 3.8D-F**), the UV/vis data of Y48/H20 and Y108 are consistent with a change in the polarity of the environment surrounding the phenol group. This effect is confirmed in the case of Y48/H20 from the previously characterized X-ray structure.[7] From this structure (**Figure 3.2C**), the oxygen from the Y48 phenol group directly hydrogen bonds to the engineered histidine that was substituted in isoleucine.

The high-resolution X-ray structure of Y48 was collected as mentioned above for the F110L/F110A. While the Y48 participates in hydrogen bonding with histidine in Y48/H20, the structure of Y48 has no proton acceptor (**Figure 3.7E**). Further, there are no indications for any water molecules penetrating the azurin cavity. The Tm from the DSC supports that this protein variant is quite stable and comparable to that of W48. Taken together with the UV/vis data (**Figure 3.8**), Y48 azurin is in well-folded, low dielectric protein environment.

Reduction potentials of the tyrosine mutants were collected by SWV at pH 7 and pH 9-11. The potentials were collected at pH 7 to compare to the tryptophan mutants. Y48 had a higher reduction potential than W48. At pH 9, the potential of Y48 was significantly lower than Y48/H20. Note that the Y48/H20 protein variant becomes unstable at reduced (neutral or lower) pH values as the histidine becomes protonated. The hydrogen bond therefore made it less favorable for reduction to occur. The trend of hydrogen bonding elevating the reduction potentials aligns with that discussed above for the tryptophan variants, with the higher the polarity being linked to a higher reduction potential.

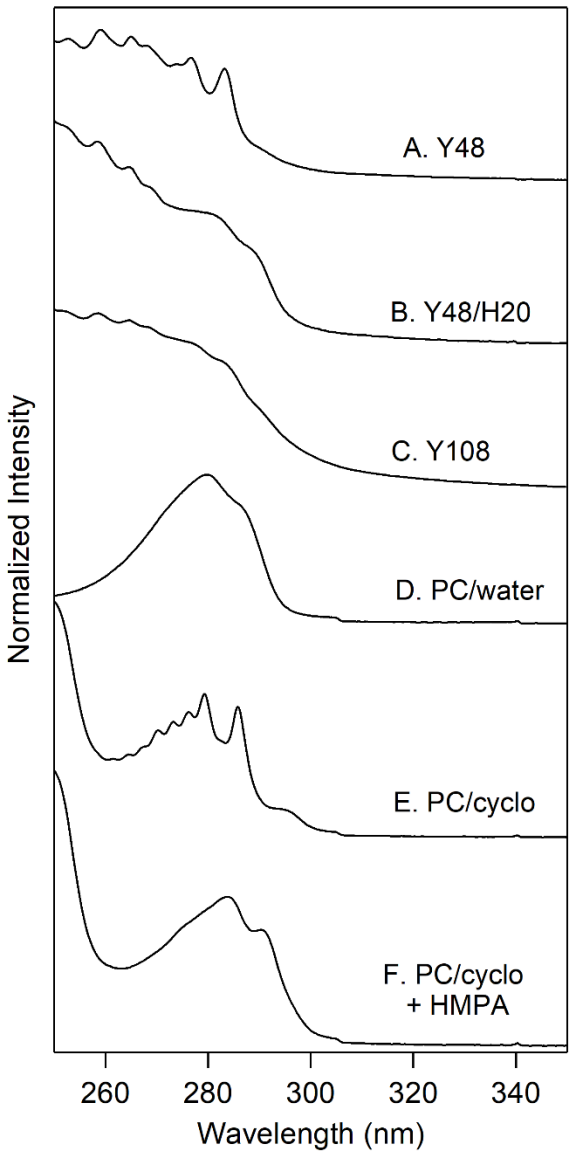

Figure 3.8. UV/vis spectra of Y azurin variants (A-C) and p-cresol in various solvents (D-F). Azurin solutions were prepared at 10 μM in 25 mM phosphate, pH 7. The concentration of the p-cresol was 200 μM. The spectra were normalized for the peak absorbance at ~280 nm.

References

1. Barry, B. A.; Chen, J.; Keough, J.; Jenson, D.; Offenbacher, A.; Pagba, C., Proton-Coupled Electron Transfer and Redox-Active Tyrosines: Structure and Function of the

Tyrosyl Radicals in Ribonucleotide Reductase and Photosystem II. *J. Phys. Chem. Lett.* **2012**, *3*, 543-554.

2. Stubbe, J.; van der Donk, W. A., Protein Radicals in Enzyme Catalysis. *Chem. Rev.* **1998**, *98*, 705-762.
3. Gray, H. B.; Winkler, J. R., Hole Hopping through Tyrosine/Tryptophan Chains Protects Proteins from Oxidative Damage. *Proc. Natl. Acad. Sci. U.S.A.* **2015**, *112*, 10920-10925.
4. Greene, B. L.; Kang, G.; Cui, C.; Bennati, M.; Nocera, D. G.; Drennan, C. L.; Stubbe, J., Ribonucleotide Reductases: Structure, Chemistry, and Metabolism Suggest New Therapeutic Targets. *Annu. Rev. Biochem.* **2020**, *89*, 45-75.
5. Weinberg, D. R.; Gagliardi, C. J.; Hull, J. F.; Murphy, C. F.; Kent, C. A.; Westlake, B. C.; Paul, A.; Ess, D. H.; McCafferty, D. G.; Meyer, T. J., Proton-Coupled Electron Transfer. *Chem. Rev.* **2012**, *112*, 4016-4093.
6. Tyson, K. J.; Davis, A. N.; Norris, J. L.; Bartolotti, L.; Hvastkovs, E. G.; Offenbacher, A. R., Impact of Local Electrostatics on the Redox Potentials of Tryptophan Radicals in Azurin: Implications for Redox-Active Tryptophans in Proton-Coupled Electron Transfer. *J. Phys. Chem. Lett.* **2020**, *11*, 2408-2413.
7. Warren, J. J.; Winkler, J. R.; Gray, H. B., Redox Properties of Tyrosine and Related Molecules. *FEBS Letters* **2012**, *586*, 596-602.
8. Hammann, C.; Messerschmidt, A.; Huber, R.; Nar, H.; Gilardi, G.; Canters, G. W., X-Ray Crystal Structure of the Two Site-Specific Mutants Ile7ser and Phe110ser of Azurin from Pseudomonas Aeruginosa. *J. Mol. Biol.* **1996**, *255*, 362-366.

9. Gabellieri, E.; Balestreri, E.; Galli, A.; Cioni, P., Cavity-Creating Mutations in Pseudomonas Aeruginosa Azurin: Effects on Protein Dynamics and Stability. *Biophys. J.* **2008**, *95*, 771-781.
10. La Rosa, C.; Milardi, D.; Grasso, D.; Guzzi, R.; Sportelli, L., Thermodynamics of the Thermal Unfolding of Azurin. *J. Phys. Chem.* **1995,** *99*, 14864-14870.
11. Guzzi, R.; Sportelli, L.; La Rosa, C.; Milardi, D.; Grasso, D.; Verbeet, M. P.; Canters, G. W., A Spectroscopic and Calorimetric Investigation on the Thermal Stability of the Cys3ala/Cys26ala Azurin Mutant. *Biophys. J*. **1999**, *77*, 1052-1063.
12. Westerlund, K.; Moran, S. D.; Privett, H. K.; Hay, S.; Jarvet, J.; Gibney, B. R.; Tommos, C., Making a Single-Chain Four-Helix Bundle for Redox Chemistry Studies. *Protein Eng. Des. Sel*. **2008**, *21*, 645-652.
13. Glover, S. D.; Tyburski, R.; Liang, L.; Tommos, C.; Hammarstrom, L., Pourbaix Diagram, Proton Coupled Electron Transfer, and Decay Kinetics of a Protein Tryptophan Radical: Comparing the Redox Properties of W32 and Y32 Generated inside the Structurally Characterized A3w and A3y Proteins. *J. Am. Chem. Soc*. **2018**, *140*, 185-192.
14. Nar, H.; Huber, R.; Messerschmidt, A.; Filippou, A. C.; Barth, M.; Jaquinod, M.; Van De Kamp, M., Characterization and Crystal Structure of Zinc Azurin, a by-Product of Heterologous Expression in Escherichia Coli of Pseudomonas Aeruginosa Copper Azurin. *Eur. J. Biochem*. **1992**, *205*, 1123.
15. Vaitheeswaran, S.; Yin, H.; Rasaiah, J. C.; Hummer, G., Water Clusters in Nonpolar Cavities. *Proc. Natl. Acad. Sci. U.S.A.* **2004**, *101*.

16. Biedermann, F.; Nau, W. M.; Schneider, H. J., The Hydrophobic Effect Revisited - Studies with Supramolecular Complexes Imply High Energy Water as Noncovalent Driving Force. *Angew. Chem.* **2014**, *53*, 11158-11171.

Chapter 4: Conclusion

Past research has been performed on measuring the reduction potentials of tryptophan and tyrosine in peptide and mock-protein environments. This research was primarily done to determine the impact of sequestering the amino acids from solvent into a protein environment, on the reactivity of amino acids in mediating proton-coupled electron transfer (PCET). However, little was known about how variable environmental changes would impact reduction potentials in a larger, complex protein environment with variable dielectrics. This thesis addressed these research gaps by investigating the sensitivity of reduction potentials of tyrosine and tryptophan in variable protein environments using the model protein, azurin. With its native sequence containing a single tryptophan residue and two tyrosine residues, Azurin was relatively easy to mutate to achieve isolation of one redox active amino acid. From this system as a starting point, two positions (W/Y48 or W/Y108) were created to compare a solvent excluded environment and a solvent exposed one, respectively. The reduction potentials were seen to respond to the degree of solvent exposure. Further strategic mutations were later performed on the non-polar W/Y48 proteins that altered the central cavity size, the polarity of the environment, and the ability to hydrogen bond. pH studies were also performed to monitor pK_a and other thermodynamic variables.

It was discovered that the W108 protein had a reduction potential of approximately 100 mV higher than the W48 protein, indicating that exhibited hydrogen bonding with the surrounding solvent to which it was exposed to. W48 was solvent excluded and surrounded by a non-polar environment, in comparison. Y48 also had a higher reduction potential than W48, but only by about 20 mV. The two were experiencing the same local environments, and while the polarity of the two are different, they were not different enough to create a significant potential difference.

The W48 protein was further studied by performing local mutations to the F110 amino acid which was directly across from the W48 in the natural protein.

Overall, this thesis provides important information regarding the impact of protein environmental modifications on reduction potentials of tryptophan and tyrosine. The knowledge gained from this project can be used to assist in protein design and engineering as the control of PCET is critical for biocatalytic processes. For example, ribonucleotide reductase is a large, complex enzyme that reduces RNA to DNA. The reduction of RNA to DNA is incredibly important for repairing damaged DNA. This process is achieved by a cascade of electron transfer events that involve multiple tyrosine residues and a tryptophan residue. By increasing our knowledge about the environmental impacts on reduction potentials, we can begin to understand and control the thermodynamic forces of proton-coupled electron transfer. Understanding this complex control can be exploited for the rational design of oxidoreductases that use PCET coupled to catalysis.